LANGMUIR

pubs.acs.org/Langmuir Article

Effect of Ionic Strength, Nanoparticle Surface Charge Density, and Template Diameter on Self-Limiting Single-Particle Placement: A Numerical Study

Pushkar K. Gothe, Anthony Martinez, and Seong Jin Koh*



Cite This: *Langmuir* 2021, 37, 11961–11977



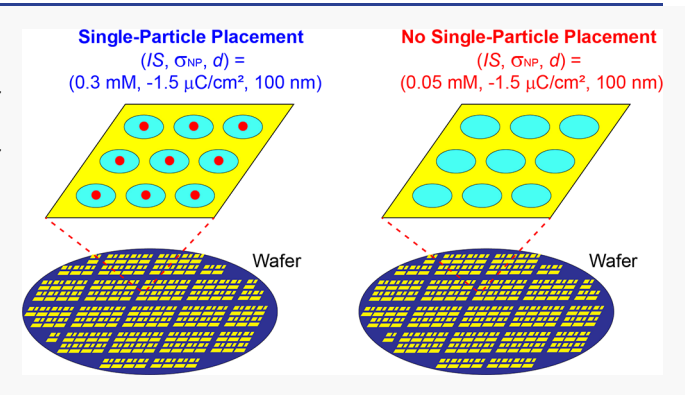
ACCESS I

III Metrics & More

Article Recommendations

S Supporting Information

ABSTRACT: For the bottom-up approach where functional materials are constructed out of nanoscale building blocks (e.g., nanoparticles), it is essential to have methods that are capable of placing the individual nanoscale building blocks onto exact substrate positions on a large scale and on a large area. One of the promising placement methods is the self-limiting single-particle placement (SPP), in which a single nanoparticle in a colloidal solution is electrostatically guided by electrostatic templates and exactly one single nanoparticle is placed on each target position in a self-limiting way. This paper presents a numerical study on SPP, where the effects of three key parameters, (1) ionic strength (IS), (2) nanoparticle surface charge density $(\sigma_{\rm NP})$, and (3) circular template diameter (d), on SPP are investigated. For 40 different



parameter sets of (IS, σ_{NP} , d), a 30 nm nanoparticle positioned at \vec{R} above the substrate was modeled in two configurations (i) without and (ii) with the presence of a 30 nm nanoparticle at the center of a circular template. For each parameter set and each configuration, the electrostatic potentials were calculated by numerically solving the Poisson-Boltzmann equation, from which interaction forces and interaction free energies were subsequently calculated. These have identified realms of parameter sets that enable a successful SPP. A few exemplary parameter sets include (IS, σ_{NP} , d) = (0.5 mM, $-1.5 \mu C/cm^2$, 100 nm), (0.05 mM, $-0.5 \mu C/cm^2$, 100 nm), (0.5 mM, $-1.5 \mu C/cm^2$, 150 nm), and (0.05 mM, $-0.8 \mu C/cm^2$, 150 nm). This study provides clear guidance toward experimental realizations of large-scale and large-area SPPs, which could lead to bottom-up fabrications of novel electronic, photonic, plasmonic, and spintronic devices and sensors.

■ INTRODUCTION

Nanoscale entities, such as metal nanoparticles, semiconductor quantum dots, dielectric nanoparticles, and magnetic nanoparticles (here, we collectively call them nanoparticles), have been the subjects of intensive studies due to their novel electrical, optical, and magnetic properties that their bulk counterparts cannot provide. Their unique properties and applications include atom-like energy levels, ¹⁻³ Coulomb blockade in single-electron transport, ³⁻⁹ single-photon sources, ^{10,11} on-demand generation of entangled photon pairs, ^{11,12} plasmonics, ¹³⁻²³ surface plasmon amplification by the stimulated emission of radiation (spaser), ²⁴⁻²⁶ spaser nanoparticle laser, ²⁴ magnetic dipole resonances in the visible spectral range, ^{27,28} and catalysts. ²⁹ To implement these in practical integrated systems, however, it is essential to have reliable methods that can controllably place those single nanoparticles onto the desired substrate positions with nanoscale precision.

Various methods have been investigated for controlled placement of nanoparticles.^{30–32} These include particle assembly using capillary forces,^{31–37} placement using electro-

static interactions, ^{38–50} electrophoresis-assisted placement, ^{50,51} chemically directed nanoparticle assembly, ⁵² placing single nanoparticles using optical forces, ^{53–56} self-assembly of Au nanoparticles using highly specific protein pairing, ^{57,58} DNA-assisted nanoparticle self-assembly and placement, ^{21,59–62} formation of nanoparticle arrays assisted by block copolymers, ^{63,64} nanoparticle assembly using magnetic forces, ⁶⁵ single-nanoparticle positioning with atomic force microscopy (AFM), ⁶⁶ and pick-and-place technique for integrating quantum dots into waveguides. ^{11,67,68}

An ideal nanoparticle placement method would have the following capabilities: (1) placing individual single nanoparticles on the targeted positions with nanoscale precision, (2) parallel processing that allows single nanoparticles to be

Received: May 23, 2021
Revised: September 22, 2021
Published: October 6, 2021





placed on a large scale and a large area (e.g., on a wafer scale), and (3) the nanoparticle placement can be completed in a short time (e.g., in 5 min). One of the promising approaches that can provide all the above capabilities is the self-limiting single-particle placement (SPP), in which single nanoparticles are electrostatically guided toward target positions and exactly one single nanoparticle is placed at each target position.³⁹ Figure 1 shows a schematic of SPP. Circular templates are

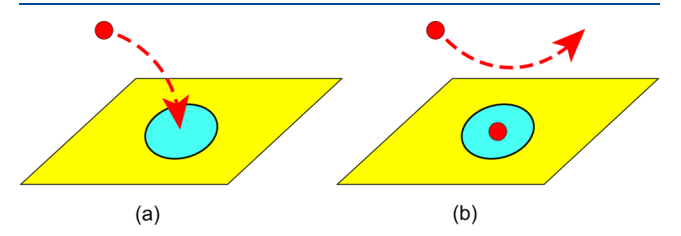


Figure 1. Schematic of self-limiting SPP (ref 39). Inside and outside of the circle are positively and negatively charged, respectively. Nanoparticle (red dot) is negatively charged. (a) A nanoparticle (in a colloidal solution) is electrostatically guided toward the circle center. (b) Once nanoparticle is placed at the circle center, the approach of other nanoparticles toward the circular template is prohibited. Reprinted from ref 39, with the permission of AIP Publishing.

made on a substrate, and positively and negatively charged self-assembled monolayers (SAMs) are formed inside and outside of the circular templates, respectively. When a colloid of negatively charged nanoparticles is applied onto the substrate, a single nanoparticle is electrostatically guided toward the circle center through electrostatic funneling³⁸ and placed at the circle center, as shown in Figure 1a. Once a nanoparticle is placed at the circle center, the electrostatic landscape changes such that it prevents the approach of other nanoparticles toward the circular template, resulting in self-limiting SPP, as shown in Figure 1b.

The key merits of this SPP method are that (1) exactly one single nanoparticle can be placed for each circular template and the circular templates can be made at any regular or irregular user-defined locations on a substrate, (2) the circular templates (diameter: ~100 nm) can be defined on a wafer scale using photolithography, (3) the electrostatic funneling mechanism (focusing effect)³⁸ enables an extremely high placement precision (~10 nm), and (4) the nanoparticle placement process is very fast.

To fully utilize the above merits of SPP, it is essential to systematically study the effects of various parameters that influence SPP. The parameters include ionic strength (IS) of the nanoparticle colloid, pH of the colloid, circular template diameter (d), and surface charge densities of the nanoparticle (σ_{NP}) , the circular template $(\sigma_{\mathrm{circle}})$, and the substrate $(\sigma_{
m substrate}).$ The effects of these parameters on SPP are entangled and rather complex. For example, increasing nanoparticle surface charge densities increases the attractive forces between a nanoparticle and the circular template but also increases the repulsive forces between the nanoparticle and the substrate surface. The magnitudes of these forces depend on the ionic strength as well as the size of the circular template. Considering this complexity, investigating the effect of many parameters on SPP by experiments alone would be a huge task. A theoretical study that systematically examines the effects of those parameters on SPP is much needed.

This paper presents a numerical study that investigates the effect of three important parameters on the characteristics of SPP. These parameters are ionic strength (IS), nanoparticle surface charge density (σ_{NP}) , and the diameter of the circular template (d). The ranges of parameter values explored are selected to closely represent the experimental conditions. Their values are from 0.05 to 0.5 mM for IS, from -0.3 to $-3.0 \mu C/$ cm² for σ_{NP}^{69-72} and 100 and 150 nm for d. By solving the Poisson-Boltzmann equation (PBE)^{39,73} for a given parameter set (IS, σ_{NP} , d), we calculate the interaction force and interaction free energy when a single nanoparticle that approaches the substrate is at a position R without and with the presence of a nanoparticle at the center of the circular template. For each parameter set (IS, σ_{NP} , d), the free energy barrier against the approaching single nanoparticle is evaluated. The magnitudes of the free energy barriers without and with the presence of a nanoparticle at the circle center determine whether the specific parameter set provides conditions for successful SPP. This numerical study provides a systematic understanding for the roles of ionic strength, nanoparticle surface charge density, and the template diameter on the selflimiting SPP and identifies the realms of the parameter space that enable successful SPP.

METHODOLOGY

Configurations. The geometrical configurations for calculating electrostatic potentials, interaction forces, and

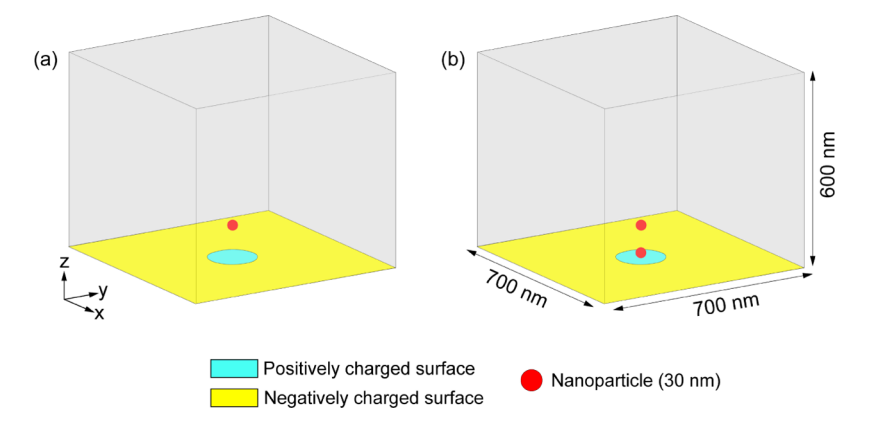


Figure 2. Geometrical configurations for solving the PBE. (a) Without the presence of a nanoparticle at the circle center. (b) With the presence of a nanoparticle at the circle center. The reference coordinate (0, 0, 0) is at the center of the circular template. The nanoparticle at the circular template is positioned at (0, 0, 15 nm). The diameter of the circular template: 100 nm or 150 nm.

interaction free energies are shown in Figure 2, one for the case that there is no nanoparticle at the circle center (Figure 2a) and the other that there is a nanoparticle at the circle center (Figure 2b). Each calculation volume has x, y, and zdimensions of 700, 700, and 600 nm, respectively. We define the center of the circular template on the substrate as the geometrical reference point (0, 0, 0). Spherical nanoparticles with a diameter of 30 nm were used as model nanoparticles. The surface charge densities of 0.42 and $-0.62 \mu C/cm^2$ were used inside and outside of the circular template, respectively (see Supporting Information).^{74–76} These values were selected to represent the experimental conditions, where SAMs of 3aminopropyltriethoxysilane (APTES: terminated by $-NH_3^+$) and 16-mercaptohexadecanoic acid (MHA: terminated by -COO⁻) are employed to make the surfaces positively and negatively charged, respectively. 74-78 A pH of 6.5 was used, where APTES SAMs are positively charged and MHA SAMs are negatively charged.^{74–77,79}

Electrostatic Potentials, Interaction Forces, and Interaction Free Energies. For a given geometry (Figure 2a or b) with a migrating nanoparticle positioned at $\vec{R} = (x, y, z)$ and for a particular parameter set of (IS, $\sigma_{\rm NP}$, d), the electrostatic potentials $\psi(\vec{r})$ are calculated by numerically solving the PBE^{39,73,80}

$$\nabla^2 \psi(\vec{r}) = -\frac{e}{\varepsilon_r \varepsilon_0} \sum_i z_i \rho_{0i} \exp(-z_i \varepsilon \psi(\vec{r})/kT)$$
(1)

where e is the unit charge of an electron, ε_r is the dielectric constant of water, ε_0 is the permittivity of the free space, z_i is the valency of ion species i, ρ_{0i} is the concentration of ion species i in the bulk, k is the Boltzmann constant, and T is the absolute temperature. COMSOL Multiphysics software was used to numerically solve the non-linear PBE, eq. 1.

Once the electrostatic potentials $\psi(\vec{r})$ are obtained, the interaction force $\vec{F}(\vec{R})$ exerted on the nanoparticle positioned at \vec{R} is calculated through $^{39,80-84}$

$$\vec{F}(\vec{R}) = \int \int_{S} \left[\left(kT \sum_{i} (\rho_{i} - \rho_{0i}) \right) \mathbf{I} \cdot \hat{n} + \left(\frac{\varepsilon_{0} \varepsilon_{r}}{2} |\vec{E}|^{2} \mathbf{I} \cdot \hat{n} \right) \right] dS$$

$$- \varepsilon_{0} \varepsilon_{r} (\vec{E} \cdot \hat{n}) \vec{E} dS$$
(2)

with $\rho_i(\vec{r}) = \rho_{0i} \exp(-z_i e \psi(\vec{r})/kT)$ and $\vec{E}(\vec{r}) = -\nabla \psi(\vec{r})$.

Here, $\rho_i(\vec{r})$ is the concentration of ion species i at a vector point \vec{r} , $\vec{E}(\vec{r})$ is the electric field, \vec{I} is the unit tensor, and \hat{n} is the unit vector pointing normal to surface S enclosing the nanoparticle at \vec{R} . Surface S can be any surface that encloses the nanoparticle, S^{0-84} for which we used the surface of a hypothetical sphere whose center is at the nanoparticle position \vec{R} with a radius of 25 nm.

The interaction free energies $\vec{V}(\vec{R})$ are calculated by integrating the interaction forces $\vec{F}(\vec{R})$ through $^{39,81-84}$

$$V(\vec{R}) = -\int \vec{F}(\vec{Q}) \cdot d\vec{Q}$$
(3)

The reference interaction free energy was defined as the interaction free energy when the nanoparticle is positioned far above the substrate, at $\vec{R} = (0, 0, 350 \text{ nm})$; V(0, 0, 350 nm) = 0

Surface Charge Densities, Stern Potentials, and Boundary Conditions for PBE. We define the surface

charge density σ as the total charge in the Stern layer per unit area [i.e., the charge at the inner Helmholtz plane (IHP) plus that at the outer Helmholtz plane (OHP) per unit area]. 71,75,76 Due to the charge neutrality, the surface charge density σ is the same as the integrated charge density of the diffuse layer $\sigma_{\rm d}$ with the opposite polarity ($\sigma = -\sigma_{\rm d}$). The charge density $\sigma_{\rm d}$ of the diffuse layer is directly related to the Stern potential $\psi_{\rm d}$ at the outer Helmholtz plane (OHP: the boundary of the diffuse layer and the Stern layer). Their relationship is obtained by solving the PBE in the diffuse layer. The OHP is located very close to the slip plane and we assume that the Stern potential $\psi_{\rm d}$ at the OHP is equal to the zeta potential ζ at the shear plane. 71,75,76,85–88 Various techniques can be used to experimentally measure the zeta potentials ζ , 71,75,89–92 from which the values of the surface charge density σ are obtained from the $\psi_{\rm d}$ - σ relationship (with $\psi_{\rm d} = \zeta$).

At a given pH, the surface charge density σ of a given surface remains the same even when the ionic strength (IS) varies, while its Stern potential $\psi_{\rm d}$ does change with varying ionic strengths. For each surface charge density $\sigma_{\rm NP}$, $\sigma_{\rm circle}$, and $\sigma_{\rm substrate}$ of the nanoparticle, circular template, and substrate surface, respectively, their Stern potentials $\psi_{\rm NP}$, $\psi_{\rm circle}$, and $\psi_{\rm substrate}$ have been calculated for varying ionic strengths (see Supporting Information). These are summarized in Table S4 in Supporting Information.

We use Dirichlet boundary conditions (i.e., maintaining a constant potential at each boundary) in numerically solving the PBE. The Stern potentials $\psi_{\rm NP}$, $\psi_{\rm circle}$, and $\psi_{\rm substrate}$ in Table S4 have been used for the Dirichlet boundary conditions for specific $\sigma_{\rm NP}$, $\sigma_{\rm circle}$, and $\sigma_{\rm substrate}$ at a given ionic strength (*IS*) and at pH 6.5. For *IS* = 0.05 mM, as an example, a set of the surface charge densities ($\sigma_{\rm NP}$, $\sigma_{\rm circle}$, $\sigma_{\rm substrate}$) = (-0.50 μ C/cm², 0.42 μ C/cm², -0.62 μ C/cm²) provides a set of Stern potentials ($\psi_{\rm NP}$, $\psi_{\rm circle}$, $\psi_{\rm substrate}$) = (-76.0 mV, 118.6 mV, -138.2 mV) (see Table S4). These Stern potential values are used for the Dirichlet boundary conditions for nanoparticle, circular template, and substrate surface. All calculations are carried out at 295 K.

When two surfaces get very close to each other (<~Debye length), charge redistribution of the surfaces [charge regulation (CR) needs to be accounted for and the accuracy of using the Dirichlet boundary condition [constant potential (CP)] needs to be evaluated. 93-96 It is known that the values of interaction forces and interaction free energies (IFEs) calculated with the CR boundary condition lie between those calculated with the CP boundary condition and those calculated with constant charge (CC). 93,95,96 For the parameter space, we explored in this study, we find that the calculated values of interaction forces and IFEs with CP and CC boundary conditions are very similar to each other, with some deviation for the lowest ionic strength of 0.05 mM (see Section IV of the Supporting Information). This means that using either the CP or CC boundary condition serves for our purpose. We use the CP boundary condition in solving the PBE's throughout this study. The validity and limitation of using this boundary condition are discussed in Section IV of the Supporting Information.

RESULTS AND DISCUSSION

Electrostatic Potential. For a nanoparticle positioned at $\vec{R} = (x, y, z)$, we have solved the PBE (eq 1) and obtained electrostatic potentials $\psi(\vec{r})$ for varying ionic strengths (IS = 0.5, 0.3, 0.1, and 0.05 mM), nanoparticle surface charge densities ($\sigma_{\rm NP} = -3.0, -1.5, -0.8, -0.5,$ and $-0.3~\mu{\rm C/cm}^2$),

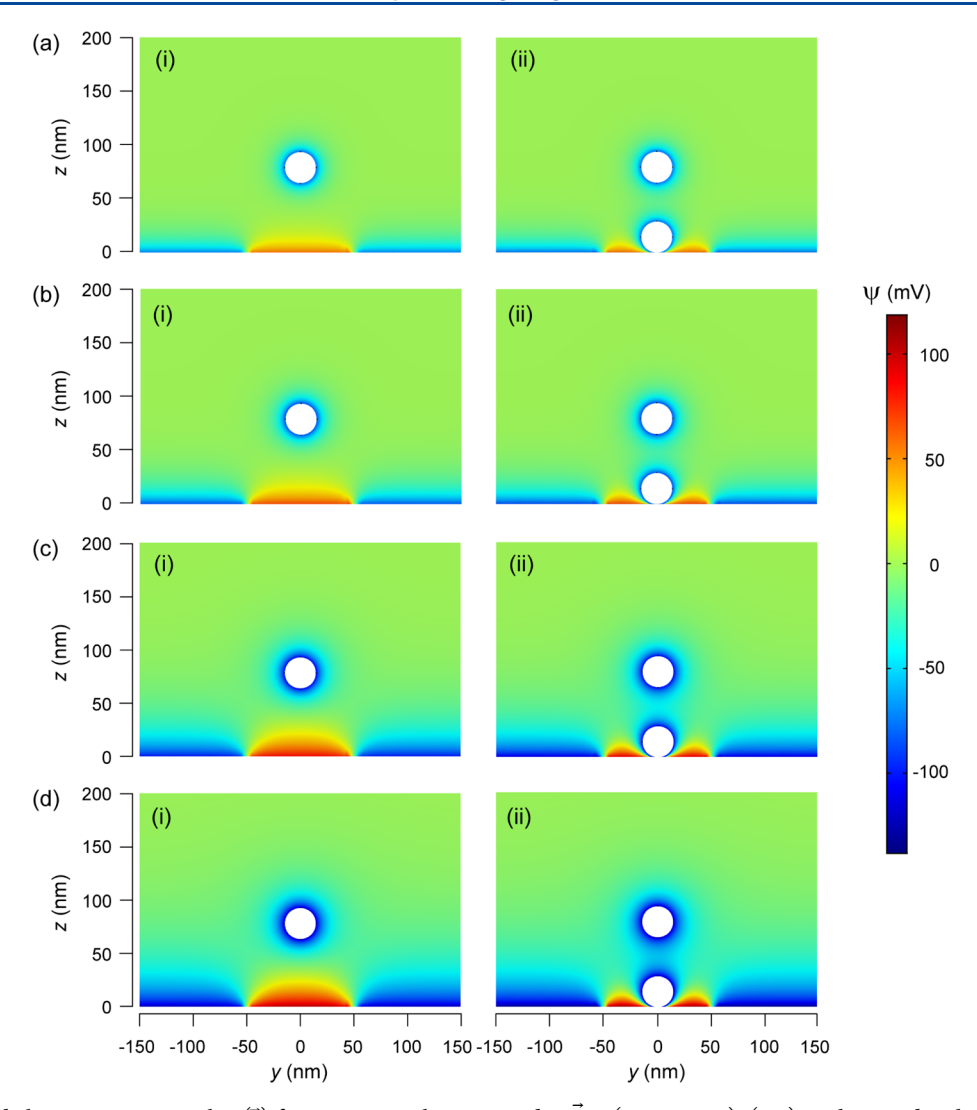


Figure 3. Calculated electrostatic potentials $\psi(\vec{r})$ for a nanoparticle positioned at $\vec{R} = (0, 0, 80 \text{ nm})$. (i, ii): without and with a nanoparticle at the circle center, respectively. (a) $(IS, \sigma_{NP}, d) = (0.5 \text{ mM}, -0.8 \,\mu\text{C/cm}^2, 100 \text{ nm})$. (b) $(IS, \sigma_{NP}, d) = (0.3 \text{ mM}, -0.8 \,\mu\text{C/cm}^2, 100 \text{ nm})$. (c) $(IS, \sigma_{NP}, d) = (0.1 \text{ mM}, -0.8 \,\mu\text{C/cm}^2, 100 \text{ nm})$. (d) $(IS, \sigma_{NP}, d) = (0.05 \text{ mM}, -0.8 \,\mu\text{C/cm}^2, 100 \text{ nm})$. For all calculations, pH = 6.5, $\sigma_{circle} = 0.42 \,\mu\text{C/cm}^2$, and $\sigma_{substrate} = -0.62 \,\mu\text{C/cm}^2$.

and diameters of the circular template (d=100 and 150 nm); for a given nanoparticle position \vec{R} , $\psi(\vec{r})$ have been evaluated for a total of 40 (= 4 × 5 × 2) different sets of (\vec{IS} , $\sigma_{\rm NP}$, d). These calculations were done for 51 different \vec{R} 's, whose positions are displayed in Figure S2 in Supporting Information. For each \vec{R} and a specific parameter set (\vec{IS} , $\sigma_{\rm NP}$, d), $\psi(\vec{r})$ were calculated for two configurations, (i) with no nanoparticle at the circle center and (ii) with a nanoparticle at the circle center.

Several of the calculated electrostatic potentials $\psi(\vec{r})$ are shown in Figure 3 as examples, where we display $\psi(\vec{r})$ for a nanoparticle positioned at $\vec{R}=(0,0,80~\text{nm})$ and for 4 different ionic strengths (IS=0.5,0.3,0.1, and 0.05 mM), with $\sigma_{\rm NP}=-0.8~\mu{\rm C/cm^2}$ and d=100~nm. Here, the effect of ionic strength on the electrostatic potentials is clearly visible. As the ionic strength (IS) reduces from 0.5 to 0.05 mM (Figure 3a–d), the regions of high negative potentials (the bluish color regions; < \sim -70 mV) adjacent to the substrate surface (outside of the circular template) and adjacent to nanoparticle surfaces become extended; see the increasing thicknesses of the bluish layers just above the substrate surface and increasing volume of

the bluish regions around nanoparticles. This behavior is consistent with the increasing Debye lengths with decreasing ionic strengths;⁷³ the Debye lengths are 13, 17, 30, and 43 nm for IS = 0.5, 0.3, 0.1, and 0.05 mM, respectively. For a low IS(e.g., IS = 0.05 mM), the extended regions of high negative potentials near the substrate surface and around the nanoparticle result in increasing repulsive interactions between the substrate and a migrating nanoparticle at R. For the case of no nanoparticle present on the circle center [case (i) in Figure 3], if those repulsive interactions are strong enough, they can outweigh the attractive interactions between the nanoparticle and the circular template (positively charged), preventing the approach of the nanoparticle toward the center of the circular template and therefore resulting in no nanoparticle placement on the circular template. For a higher ionic strength (e.g., IS =0.5 mM), the smaller Debye length leads to smaller repulsive interactions between the substrate surface and the migrating nanoparticle at \vec{R} , allowing the nanoparticle to approach the positively charged circular template.

For the case that one nanoparticle is present on the circle center [case (ii) in Figure 3], the calculated electrostatic

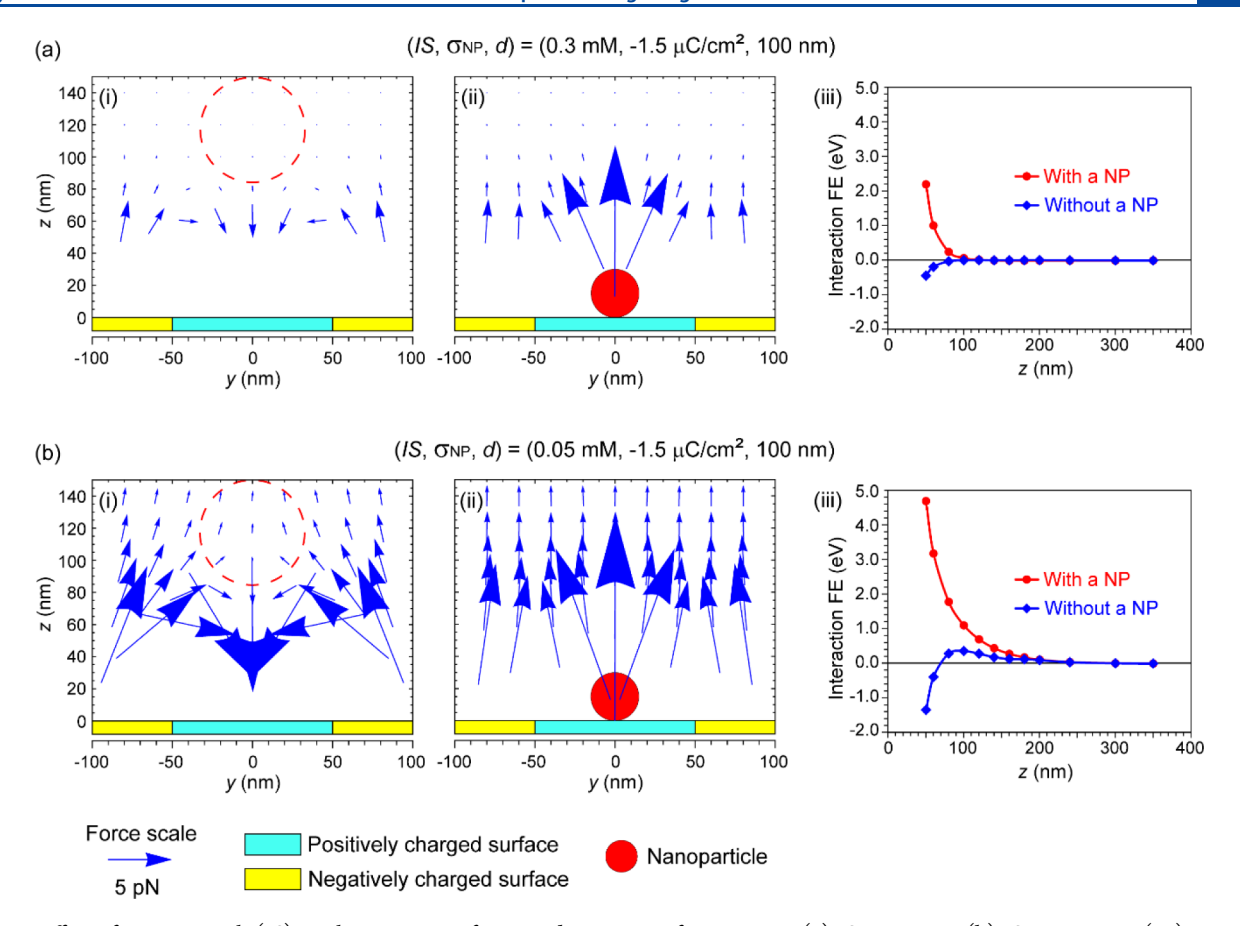


Figure 4. Effect of ionic strength (*IS*) on the interaction forces and interaction free energies. (a) IS = 0.3 mM. (b) IS = 0.05 mM. (i,ii) Interaction forces without and with a nanoparticle (NP) at the circle center, respectively. (iii) Interaction free energies as a function of z without (blue) and with (red) a nanoparticle at the circle center. pH = 6.5, $\sigma_{NP} = -1.5$ μ C/cm², $\sigma_{circle} = 0.42$ μ C/cm², $\sigma_{substrate} = -0.62$ μ C/cm².

potentials $\psi(\vec{r})$ provide the scope of the repulsive interactions between the two nanoparticles. For IS = 0.5 mM, the electrostatic potential around each nanoparticle decays fast, leaving only a thin high negative potential region (the bluish color region) around the nanoparticles and therefore resulting in only a small overlap of potential fields between the two nanoparticles, as shown in Figure 3a(ii). For lower ionic strengths, for example, IS = 0.05 mM, the electrostatic potentials around nanoparticles decay slower, resulting in a substantial overlap of the potential fields between the two nanoparticles, as shown in Figure 3d(ii). The end results of the changing landscapes of the electrostatic potentials with differing ionic strengths are that the upward repulsive force exerted on the nanoparticle at R becomes stronger as the ionic strength becomes smaller. The exact amounts of forces have been calculated from the electrostatic potentials $\psi(\vec{r})$ for different nanoparticle positions \vec{R} and different parameter sets (IS, σ_{NP} , d), which will be discussed in the following section.

Interaction Forces and Interaction Free Energies. From electrostatic potentials $\psi(\vec{r})$ and using eq 2, we have calculated the interaction forces that exert on a nanoparticle positioned at \vec{R} . These calculations have been done for the 51 different nanoparticle locations \vec{R} 's (Figure S2 in Supporting Information), each of which at the 40 different parameters sets $(IS, \sigma_{\rm NP}, d)$ and in the two configurations, (i) no nanoparticle and (ii) one nanoparticle at the center of the circular template. The calculated interaction forces are displayed in Figures S3–S12 in Supporting Information. As examples, Figure 4 shows interaction forces for two different parameters sets, $(IS, \sigma_{\rm NP}, d)$

= (0.3 mM, $-1.5 \mu C/cm^2$, 100 nm) in Figure 4a and (IS, σ_{NP} , d) = (0.05 mM, $-1.5 \mu C/cm^2$, 100 nm) in Figure 4b. Here, we examine the effect of ionic strengths (IS = 0.3 mM vs 0.05 mM) on the landscape of interaction forces. For 0.3 mM ionic strength [(IS, σ_{NP} , d) = (0.3 mM, $-1.5 \mu C/cm^2$, 100 nm)] and for the case of no nanoparticle at the circle center, as shown in Figure 4a(i), the attractive interactions between the negatively charged nanoparticle and the positively charged circular template substantially reduce the upward forces [see the forces inside the red dashed circle in Figure 4a(i)]. These reduced upward forces allow a single nanoparticle to easily approach toward the circle center, thermodynamically the most favorable site where the interaction free energy is the lowest. This facile approach of the single nanoparticle toward the circle center can be quantitatively assessed by calculating the interaction free energies using eq 3. Figure 4a(iii) shows the interaction free energies (in blue) as a function of the vertical distance (0, (0, z) from the circle center (0, 0, 0). We find that the free energy barrier (the maximum interaction free energy) is very low, only 0.009 eV, which can be easily surmountable at room temperature and therefore allow the approach of the single nanoparticle toward the circle center. Once one nanoparticle is placed at the circle center, the landscape of the interaction forces totally changes, as shown in Figure 4a(ii), where strong repulsive upward forces prohibit the second single nanoparticle from approaching toward the circular template, enabling the self-limiting SPP. This deterrence of the approach of the second nanoparticle toward the circular template can also be seen from the calculated interaction free energies in Figure

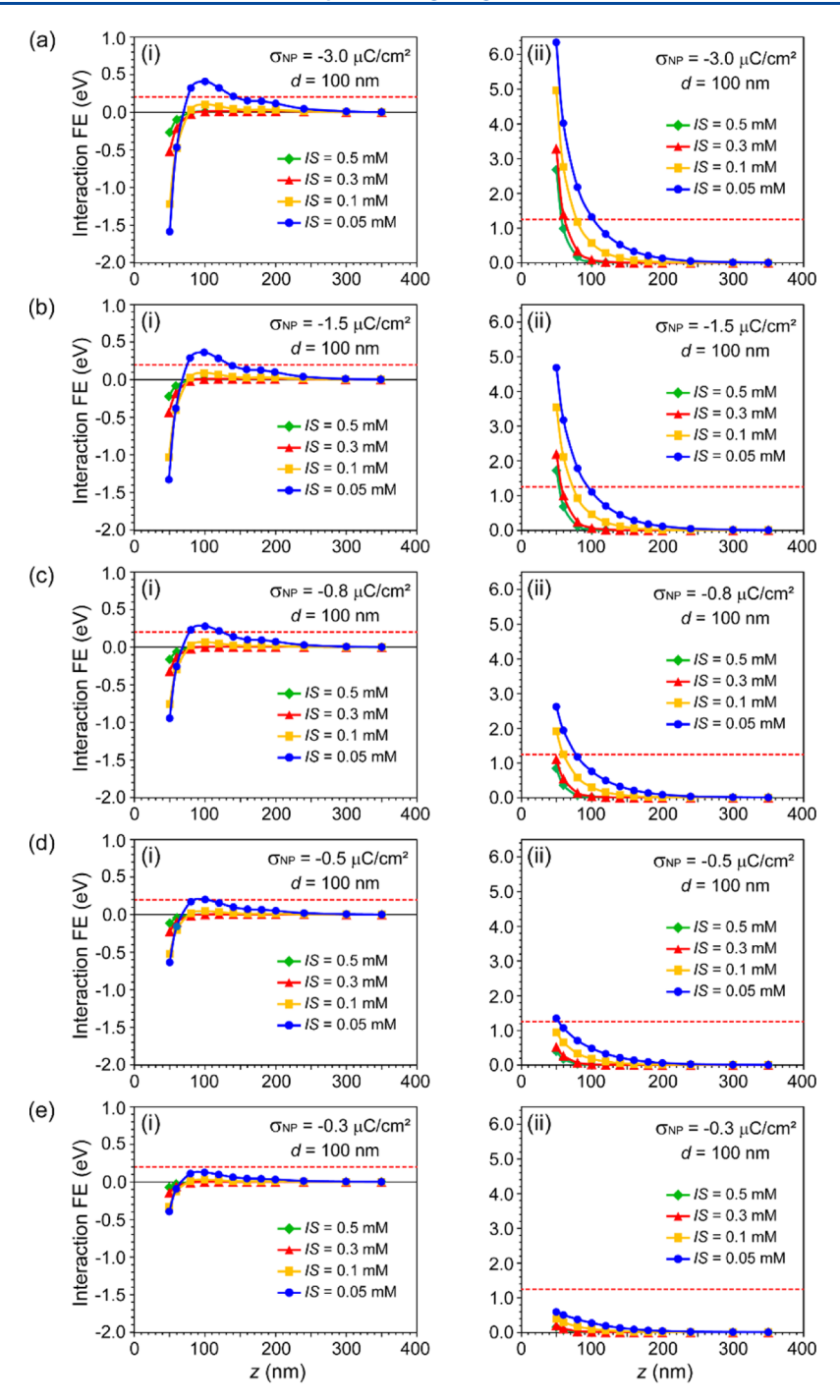


Figure 5. Effect of ionic strength on interaction free energies at various nanoparticle surface charge densities and d=100 nm. Parameters: pH = 6.5, $\sigma_{\rm circle}=0.42~\mu{\rm C/cm}^2$, and $\sigma_{\rm substrate}=-0.62~\mu{\rm C/cm}^2$. Position of the migrating nanoparticle $\vec{R}=(0,0,z)$. z is the distance from the substrate surface. The origin (0,0,0) is at the circle center. (i,ii) Without and with a nanoparticle at the circle center, respectively. The red dotted lines in (i,ii) represent the two criteria, which are 0.2 eV and 1.25 eV, respectively. (a) For $\sigma_{\rm NP}=-3.0~\mu{\rm C/cm}^2$. (b) For $\sigma_{\rm NP}=-1.5~\mu{\rm C/cm}^2$. (c) For $\sigma_{\rm NP}=-0.8~\mu{\rm C/cm}^2$. (e) For $\sigma_{\rm NP}=-0.3~\mu{\rm C/cm}^2$.

4a(iii) (in red), where the interaction free energies rapidly increase as the second single nanoparticle approaches toward the already-present first nanoparticle. When the position of the second nanoparticle is at $\vec{R} = (0, 0, 50 \text{ nm})$, the interaction free energy becomes 2.198 eV, which is much larger than the room-temperature thermal energy of 0.025 eV, effectively blocking the approach of the second single nanoparticle toward the circular template. Overall, Figure 4a(i-iii) shows that the

parameter set (IS, σ_{NP} , d) = (0.3 mM, $-1.5 \mu C/cm^2$, 100 nm) provides excellent conditions for self-limiting SPP.

A quite different landscape emerges when the ionic strength changes to 0.05 mM [i.e., (IS, $\sigma_{\rm NP}$, d) = (0.05 mM, $-1.5~\mu{\rm C/cm^2}$, 100 nm)], Figure 4b. Figure 4b(i) shows the interaction forces exerted on the first single nanoparticle (i.e., with no nanoparticle present at the circle center). Here, it can be seen that compared to the 0.3 mM ionic strength in Figure 4a(i), there exist much stronger upward interaction forces, in

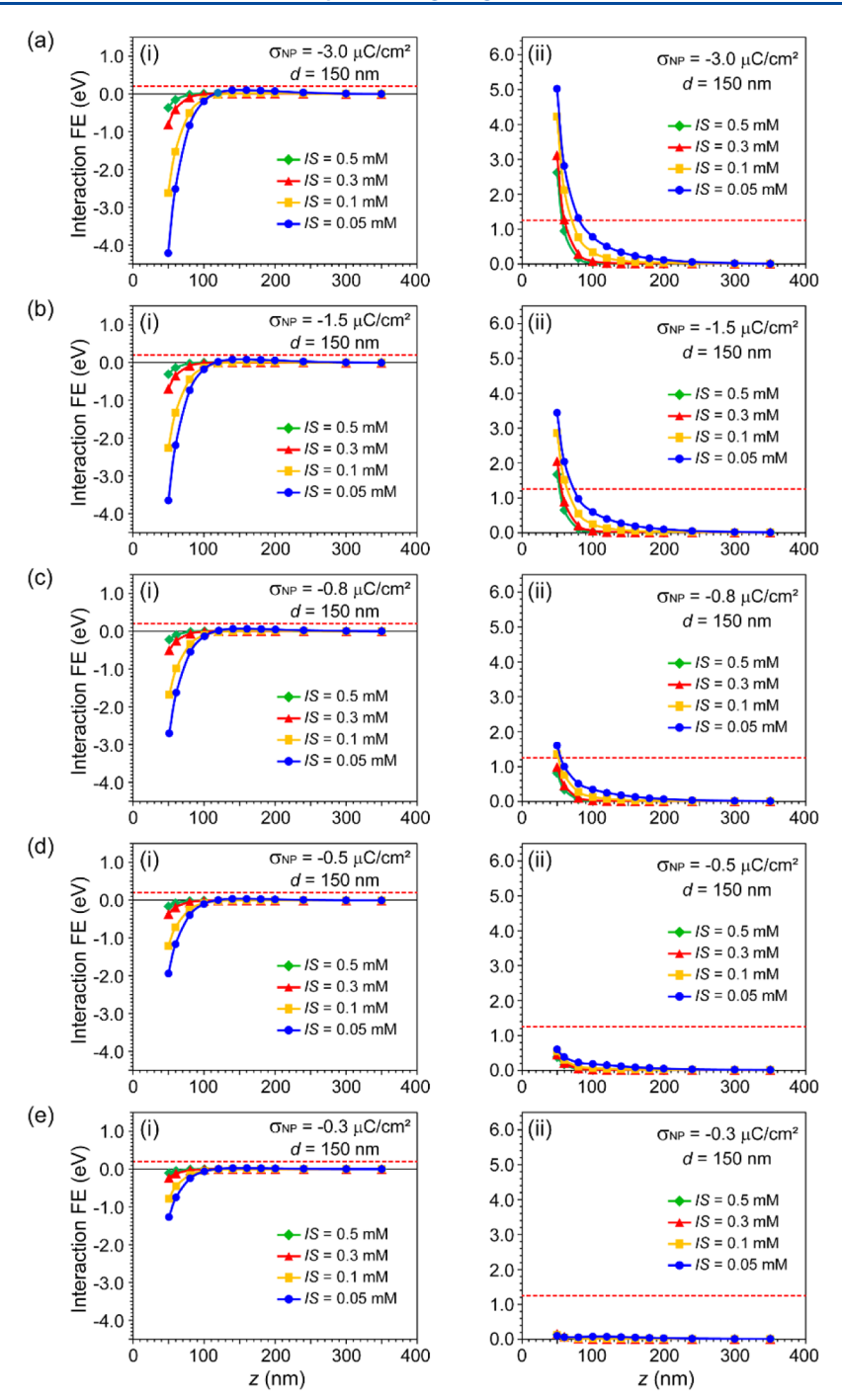


Figure 6. Effect of ionic strength on interaction free energies at various nanoparticle surface charge densities and d=150 nm. Parameters: pH = 6.5, $\sigma_{\rm circle}=0.42~\mu{\rm C/cm^2}$, $\sigma_{\rm substrate}=-0.62~\mu{\rm C/cm^2}$. Position of the migrating nanoparticle $\vec{R}=(0,0,z)$. z is the distance from the substrate surface. The origin (0,0,0) is at the circle center. (i,ii) Without and with a nanoparticle at the circle center, respectively. The red dotted lines in (i,ii) represent the two criteria, which are 0.2 and 1.25 eV, respectively. (a) For $\sigma_{\rm NP}=-3.0~\mu{\rm C/cm^2}$. (b) For $\sigma_{\rm NP}=-1.5~\mu{\rm C/cm^2}$. (c) For $\sigma_{\rm NP}=-0.8~\mu{\rm C/cm^2}$. (d) For $\sigma_{\rm NP}=-0.5~\mu{\rm C/cm^2}$. (e) For $\sigma_{\rm NP}=-0.3~\mu{\rm C/cm^2}$.

particular, when the nanoparticle is positioned above the substrate surface by 100 nm or more [see the forces in the red dashed circle in Figure 4b(i)]. These repulsive upward forces inhibit the nanoparticle from approaching toward the circular template. This inhibition can be quantitatively assessed by evaluating the interaction free energies as the nanoparticle approaches the surface, as shown in Figure 4b(iii). The interaction free energies [in blue in Figure 4b(iii)] show that there is an uphill free energy barrier of 0.362 eV as the

nanoparticle approaches toward the circle center. The 0.362 eV is much higher than the room-temperature thermal energy (0.025 eV) and the chance for a nanoparticle to overcome the free energy barrier is very low for a reasonable experimental time (e.g., 5 min). This can be seen from the following estimation. For nanoparticles in a concentration of 1 nM (the original colloid concentration), their concentration at the position where the interaction free energy is 0.362 eV is 6.57 \times 10^{-16} M (= 1.0×10^{-9} M \times $e^{-0.362 \text{eV}/kT}$, where k is the

Boltzmann constant and T is 295 K). This gives an interparticle distance (l) of 1.36×10^{-2} cm. From Stokes—Einstein equation, 97,98 a diffusion coefficient $D_{\rm NP}$ of a 30 nm nanoparticle in aqueous solution at room temperature is 1.62×10^{-7} cm²/s. Then, the time τ for a nanoparticle to overcome an interaction free energy barrier of 0.362 eV is ~ 19 min [$\tau = l^2/D_{\rm NP} = (1.36 \times 10^{-2} \ {\rm cm})^2/(1.62 \times 10^{-7} \ {\rm cm}^2/{\rm s}) \times (1 \ {\rm min/60 \ sec})$], which is longer than the 5 min of the nanoparticle placement time. Therefore, the 0.05 mM ionic strength, [(IS, $\sigma_{\rm NP}$, d) = (0.05 mM, $-1.5 \ \mu{\rm C/cm}^2$, 100 nm)], does not give a proper condition for the placement of the first nanoparticle. This is particularly true for large-scale and large-area placements for practical applications where each of the millions or billions of circular templates needs to be occupied by exactly one nanoparticle.

Although there is a very low chance that a nanoparticle can be placed at the circle center for 0.05 mM, (IS, σ_{NP} , d) = (0.05 mM, $-1.5 \mu C/cm^2$, 100 nm), we have still calculated the interaction forces and interaction free energies assuming that a nanoparticle is present at the circle center, as shown in Figure 4b(ii, iii). It can be seen that there are prominent upward repulsive forces, as shown in [Figure 4b(ii)], that extend well above 100 nm from the substrate surface. These long-range (>100 nm) upward forces prevent the second nanoparticle from approaching the substrate surface, which is also evident from the interaction free energy plot, as shown in Figure 4b(iii) (in red). Here, the free energy barrier is as high as 4.688 eV, prohibiting the approach of any second nanoparticle toward the circle center. Overall, the parameter set (IS, σ_{NP} , d) = $(0.05 \text{ mM}, -1.5 \mu\text{C/cm}^2, 100 \text{ nm})$ is not suitable for the self-limiting SPP because the 0.362 eV free energy barrier for the first single nanoparticle is too high for any single nanoparticle to reach the circular template.

The above analysis shows that for the 100 nm circle and $-1.5~\mu\text{C/cm}^2$ nanoparticle surface charge density, the 0.3 mM ionic strength provides the right conditions for the self-limiting SPP but 0.05 mM does not. Similarly, with interaction forces and interaction free energies for each of the 40 different parameter sets calculated, we can systematically analyze the effects of these parameter sets on the SPP. In particular, the analysis of the interaction free energies provides simple but quantitative criteria for effectively achieving the self-limiting SPP

Free Energy Barriers and Criteria for SPP. A self-limiting SPP can be realized when the following two conditions are satisfied. First, when the first nanoparticle approaches toward the circular template, it should experience only little or no resistance (i.e., week upward forces and small free energy barrier). Second, once the first nanoparticle is placed at the circle center, the second nanoparticle should experience large enough upward forces or a large free energy barrier, preventing the approach of the second nanoparticle toward the circular template.

In this study, we quantitatively define the above requirements by imposing two criteria on the magnitudes of the interaction free energy barriers: (1) the free energy barrier should not be larger than 0.2 eV when there is no nanoparticle at the circle center and (2) the free energy barrier should be larger than 1.25 eV when a nanoparticle is present at the circle center (for the latter, we define the free energy barrier as the free energy at z = 50 nm [the second nanoparticle is at $\vec{R} = (0, 0, 50 \text{ nm})$ although the free energies continue to increase as the second nanoparticle approaches the substrate surface].

These criteria are based on their relative magnitudes with respect to the room-temperature thermal energy, 0.025 eV. For the 0.2 eV free energy barrier for the first criterion, the time τ that a 30 nm nanoparticle to overcome a free energy barrier of 0.2 eV at room temperature can be calculated with the same procedure described earlier for a free energy barrier of 0.326 eV. The time τ for the 0.2 eV free energy barrier is calculated to be only 16 s, which is much shorter than the typical nanoparticle placement time in the experiment (e.g., 5 min). Therefore, the 0.2 eV is a low enough free energy barrier that allows the approach of the first nanoparticle toward the circle center. For the 1.25 eV free energy barrier for the second criterion, the value of $e^{-1.25 \text{eV}/kT}$ is 1.9×10^{-22} (= $e^{-1.25 \text{eV}/0.025 \text{eV}}$ = e^{-50}), meaning that it is extremely difficult for the second nanoparticle to overcome the free energy barrier in a reasonable experimental time (e.g., 5 min).

This study uses the two simple criteria above (0.2 and 1.25 eV for the free energy barriers) in determining which parameter sets are suitable for successful SPP.

Effect of Ionic Strength. We have investigated the effect of ionic strength (IS) on SPP at different nanoparticle surface charge densities ($\sigma_{NP} = -3.0, -1.5, -0.8, -0.5, \text{ and } -0.3 \,\mu\text{C}/$ cm²) and circle diameters (d = 100 and 150 nm). Figures 5 and 6 show the dependence of interaction free energies on ionic strengths for given nanoparticle surface charge densities $\sigma_{\rm NP}$ and circle diameters d. We note a few trends here. For the case that there is no nanoparticle present at the circle center [case (i) in Figures 5 and 6], as a single nanoparticle approaches toward the substrate surface (z is decreasing), the interaction free energy initially increases, reaches the maximum (the free energy barrier), and then decreases. The interaction free energy barrier is the largest at an ionic strength of 0.05 mM and it decreases as the ionic strength increases [e.g., 0.408 eV at IS = 0.05 mM and 0.012 eV at IS = 0.5 mM in Figure 5a(i)]. For the case that there is a nanoparticle present at the circle center [case (ii) in Figures 5 and 6], as a single nanoparticle approaches toward the substrate surface (z is decreasing), the interaction free energy continually increases. The magnitudes of the interaction free energies and interaction free energy barriers increase as the ionic strength decreases.

From the interaction free energy plots in Figures 5 and 6, and by imposing the two criteria defined earlier (the free energy barriers of 0.2 and 1.25 eV; indicated by red dashed horizontal lines in Figures 5 and 6), we can determine which ionic strengths are suitable for successful SPP for a given nanoparticle surface charge density $\sigma_{\rm NP}$ and a circle diameter d. For example, for $\sigma_{\rm NP} = -3.0~\mu{\rm C/cm^2}$ and $d = 100~{\rm nm}$ [Figure 5a(i,ii)], the ionic strength 0.5 mM results in a very low free energy barrier of 0.012 eV when no nanoparticle is present at the circle center [green in Figure 5a(i)] and a very high free energy barrier of 2.682 eV when a nanoparticle is present at the circle center [green in Figure 5a(ii)]. These free energy values satisfy both the two criteria, and therefore, the ionic strength 0.5 mM (with $\sigma_{\rm NP} = -3.0~\mu{\rm C/cm^2}$ and $d = 100~{\rm nm}$) provides right conditions for successful SPP. On the other hand, the ionic strength 0.05 mM results in a very high free energy barrier of 0.408 eV when no nanoparticle is present at the circle center [blue in Figure 5a(i)], which is much larger than the 0.2 eV (the first criterion) and therefore prevents the approach of the first single nanoparticle toward the circle center. Accordingly, ionic strength 0.05 mM (at $\sigma_{\rm NP} = -3.0$ μ C/cm² and d = 100 nm) does not provide right conditions for SPP.

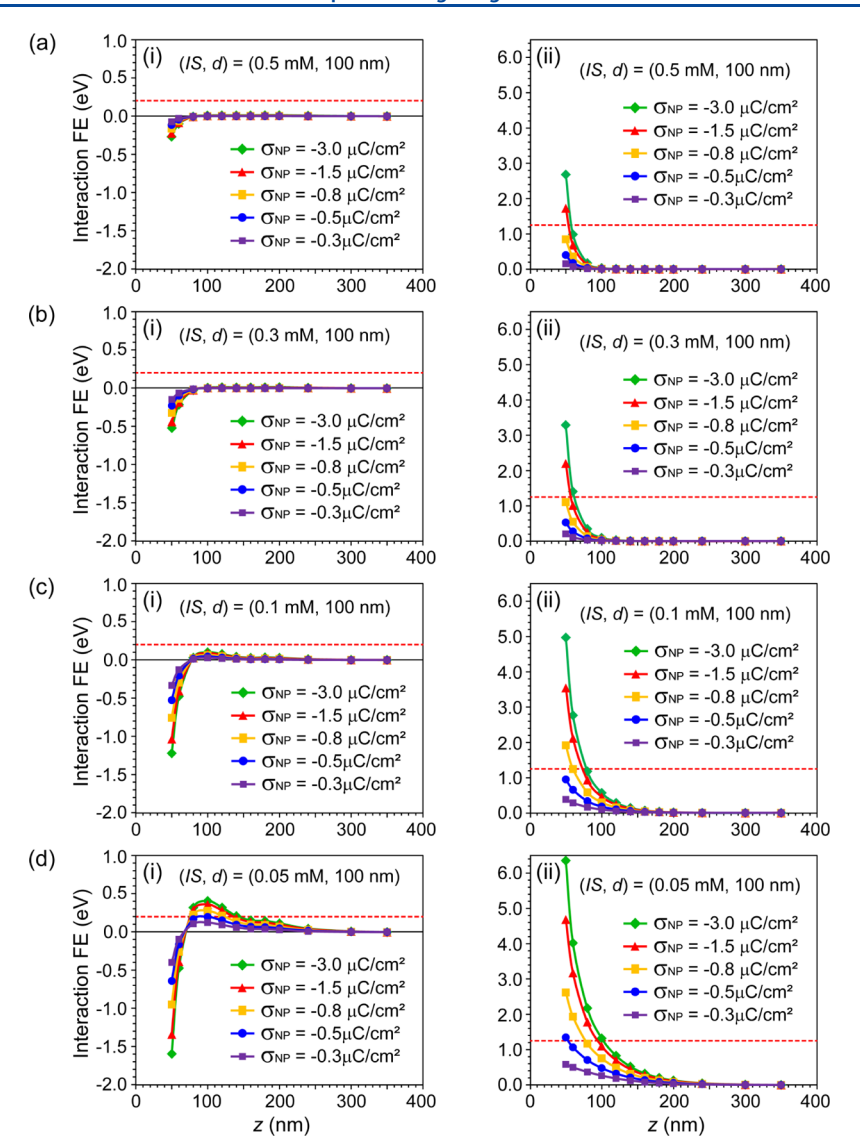


Figure 7. Effect of nanoparticle surface charge density σ_{NP} on interaction free energies at various ionic strengths and d=100 nm. Parameters: pH = 6.5, $\sigma_{circle}=0.42~\mu\text{C/cm}^2$, and $\sigma_{substrate}=-0.62~\mu\text{C/cm}^2$. Position of the migrating nanoparticle $\vec{R}=(0,0,z)$. z is the distance from the substrate surface. The origin (0,0,0) is at the circle center. (i,ii) Without and with a nanoparticle at the circle center, respectively. The red dotted lines in (i,ii) represent the two criteria, which are 0.2 and 1.25 eV, respectively. (a) For IS=0.5 mM. (b) For IS=0.3 mM. (c) For IS=0.1 mM. (d) For IS=0.05 mM.

The same analysis can be made to identify the right ionic strengths at different nanoparticle surface charge densities σ_{NP} and circle diameters d in Figures 5 and 6. For $\sigma_{\rm NP} = -3.0~\mu{\rm C}/$ cm² and d = 100 nm (Figure 5a), ionic strengths 0.5, 0.3, and 0.1 mM satisfy the two criteria. For $\sigma_{NP} = -1.5 \,\mu\text{C/cm}^2$ and d = 100 nm (Figure 5b), the ionic strengths 0.5, 0.3, and 0.1 mM also satisfy the two criteria for a successful SPP. However, the ionic strength 0.05 mM raises the interaction free energy barriers higher than the 0.2 eV [blue in Figure 5b(i)], not satisfying the first criterion. For $\sigma_{\rm NP} = -0.8 \ \mu{\rm C/cm^2}$ and d =100 nm (Figure 5c), the two criteria are satisfied only when the ionic strength is 0.1 mM. For $\sigma_{\rm NP} = -0.5 \ \mu{\rm C/cm^2}$ and d = 100nm (Figure 5d), only the ionic strength 0.05 mM (blue) satisfies the two criteria. Here, the ionic strengths 0.5 mM (green), 0.3 mM (red), and 0.1 mM (yellow) result in interaction free energy barriers of 0.395, 0.527, and 0.946 eV, respectively, with a nanoparticle present at the circle center, which are lower than the second criterion value of 1.25 eV [Figure 5d(ii)]. For $\sigma_{NP} = -0.3 \ \mu\text{C/cm}^2$ and $d = 100 \ \text{nm}$ (Figure 5e), all ionic strengths result in low free energy barriers (<0.2 eV) with no nanoparticle present at the circle center [Figure 5e(i)]. However, the interaction free energy barriers with a nanoparticle present at the circle center are lower than the 1.25 eV for all ionic strengths [Figure 5e(ii)], indicating that no IS condition is suitable for SPP when $\sigma_{\rm NP}=-0.3~\mu{\rm C/cm^2}$ and $d=100~{\rm nm}$. Figure 6 shows the effect of ionic strengths on interaction free energies when the circle diameter d is 150 nm. The same analysis can identify suitable parameter conditions for successful SPP. For $\sigma_{\rm NP}=-0.8~\mu{\rm C/cm^2}$ and $d=150~{\rm nm}$ (Figure 6c), as an example, the ionic strength 0.05 mM (blue) results in free energy barriers of 0.064 and 1.599 eV without and with the presence of a nanoparticle at the circle center, respectively, satisfying the two criteria and therefore providing suitable conditions for successful SPP.

Effect of Nanoparticle Surface Charge Density. The effect of nanoparticle surface charge densities $\sigma_{\rm NP}$ (-3.0, -1.5, -0.8, -0.5, and -0.3 $\mu{\rm C/cm^2}$) on the interaction free energies have been examined at different ionic strengths and circle

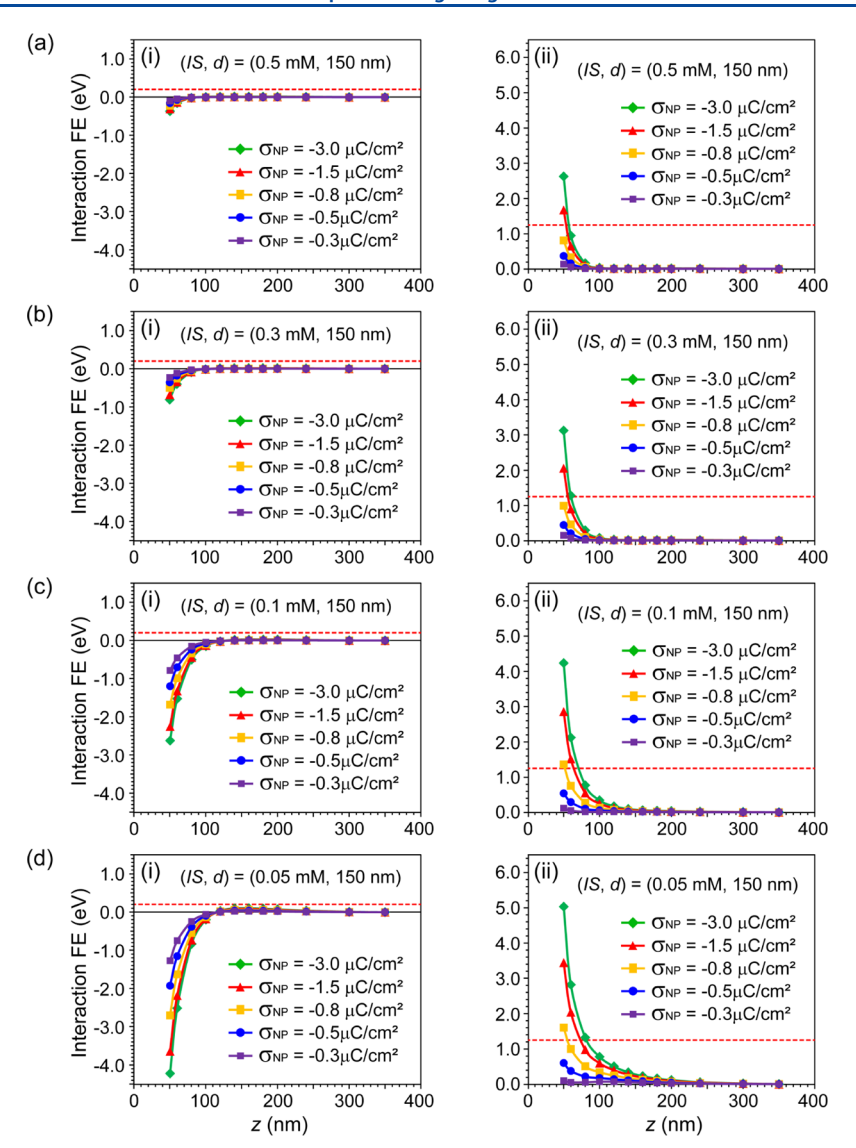


Figure 8. Effect of nanoparticle surface charge density σ_{NP} on interaction free energies at various ionic strengths and d=150 nm. Parameters: pH = 6.5, $\sigma_{circle}=0.42~\mu\text{C/cm}^2$, and $\sigma_{substrate}=-0.62~\mu\text{C/cm}^2$. Position of the migrating nanoparticle $\vec{R}=(0,0,z)$. z is the distance from the substrate surface. The origin (0,0,0) is at the circle center. (i,ii) Without and with a nanoparticle at the circle center, respectively. The red dotted lines in (i,ii) represent the two criteria, which are 0.2 and 1.25 eV, respectively. (a) For IS=0.5 mM. (b) For IS=0.3 mM. (c) For IS=0.1 mM. (d) For IS=0.05 mM.

diameters, as shown in Figures 7 and 8. For all cases in Figures 7 and 8, we observe that the magnitudes of the interaction free energies and interaction free energy barriers increase as the magnitudes of nanoparticle surface charge densities $\sigma_{\rm NP}$ increase. This dependence of interaction free energies and interaction free energy barriers on nanoparticle surface charge densities can be used to identify right parameter conditions that satisfy the two criteria for successful SPP. For IS = 0.5 mMand d = 100 nm (Figure 7a), all σ_{NP} 's result in a free energy barrier less than 0.2 eV (the first criterion) with no nanoparticle present at the circle center [Figure 7a(i)]. Once the nanoparticle is present at the circle center, only σ_{NP} 's of -3.0 and $-1.5 \mu C/cm^2$ result in a free energy barrier higher than 1.25 eV (the second criterion), Figure 7a(ii). For IS = 0.3mM and d = 100 nm (Figure 7b), all σ_{NP} 's result in low enough free energy barriers (≤0.2 eV) with no nanoparticle at the circle center [Figure 7b(i)], satisfying the first criterion. With a nanoparticle at the circle center [Figure 7b(ii)]; however, only $\sigma_{\rm NP}$'s of -3.0 and -1.5 $\mu{\rm C/cm^2}$ lead to high enough free

energy barriers (>1.25 eV) that satisfy the second criterion. Therefore, for IS = 0.3 mM and d = 100 nm, only σ_{NP} 's of -3.0and $-1.5 \mu \text{C/cm}^2$ provide the right SPP conditions that satisfy both criteria. For IS = 0.1 mM and d = 100 nm (Figure 7c), all $\sigma_{\rm NP}$'s result in low free energy barriers (≤ 0.2 eV) with no nanoparticle at the circle center [Figure 7c(i)], satisfying the first criterion. With a nanoparticle at the circle center [Figure 7c(ii)], however, only σ_{NP} 's of -3.0, -1.5, and -0.8 μ C/cm² lead to high enough free energy barriers (>1.25 eV) that satisfy the second criterion. Therefore, for IS = 0.1 mM and d = 100nm, only $\sigma_{\rm NP}$'s of -3.0, -1.5, and $-0.8~\mu{\rm C/cm^2}$ provide the right SPP conditions that satisfy both criteria. For IS = 0.05mM and d = 100 nm (Figure 7d), σ_{NP} 's of -3.0, -1.5, and $-0.8 \mu \text{C/cm}^2$ result in too high free energy barriers (>0.2 eV) with no nanoparticle present at the circle center [Figure 7d(i)], dissatisfying the first criterion. With a nanoparticle present at the circle center [Figure 7d(ii)], σ_{NP} 's of -0.3, -0.15, 0.8, and $-0.5 \mu \text{C/cm}^2$ lead to high enough free energy barriers (>1.25 eV), satisfying the second criterion. Therefore, for IS = 0.05

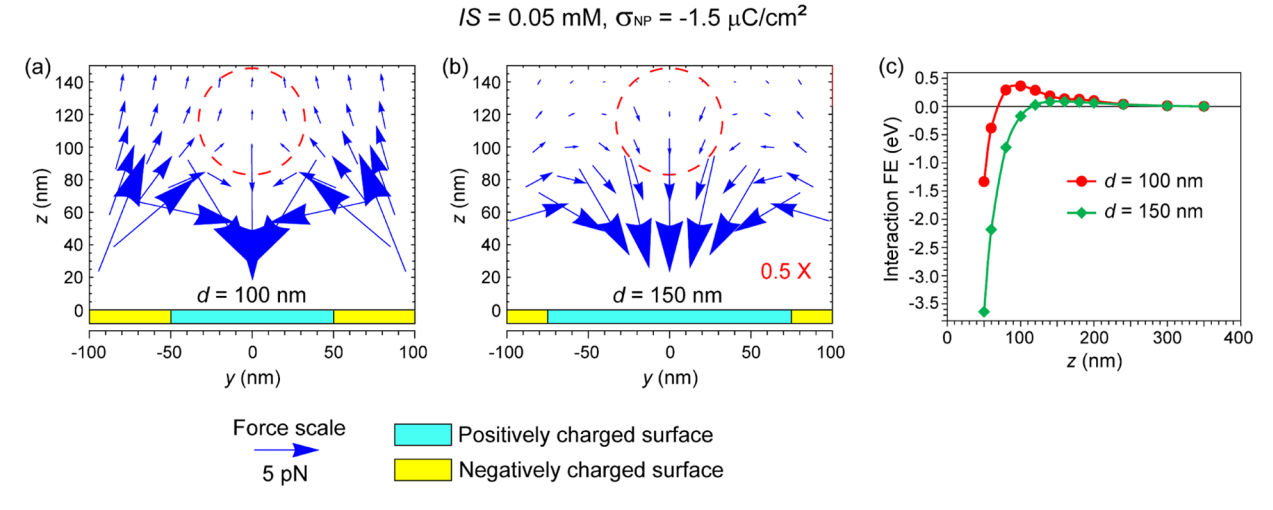


Figure 9. Effect of circle diameter on the interaction forces and interaction free energies. Parameters: pH = 6.5, IS = 0.05 mM, $\sigma_{circle} = 0.42$ μC/cm², $\sigma_{substrate} = -0.62$ μC/cm², $\sigma_{NP} = -1.5$ μC/cm². (a,b) Interaction forces for circle diameter d = 100 nm and d = 150 nm, respectively. For (b), the force arrows are in the 0.5X scale. (c) Comparison of interaction free energies (IFEs) along $\vec{R} = (0, 0, z)$ for d = 100 nm (red) and d = 150 nm (green). All are for the case that there is no nanoparticle at the circle center.

mM and d=100 nm, only $\sigma_{\rm NP}$ of $-0.5~\mu{\rm C/cm^2}$ provides the right SPP conditions. The same analysis can be made for the case of d=150 nm (Figure 8), which shows that for IS=0.5 mM (Figure 8a) and 0.3 mM (Figure 8b), $\sigma_{\rm NP}$'s of -3.0 and $-1.5~\mu{\rm C/cm^2}$ provide the right SPP conditions. For IS=0.1 mM (Figure 8c) and 0.05 mM (Figure 8d), -3.0, -1.5, and $-0.8~\mu{\rm C/cm^2}$ provide the right SPP conditions.

Effect of Circle Diameter. The effect of circle diameter on the interaction free energies can be examined by comparing the free energy data in Figures 5 and 6, as well as those in Figures 7 and 8. These show a general trend that, with other conditions the same, the smaller circle diameter (d = 100 nm) results in higher free energy barriers. This can be understood as follows. If there were no positively charged circular area (i.e., d = 0), only repulsive upward forces (due to the negatively charged substrate surface) would exert on the nanoparticle (negatively charged), leading to the highest free energy barrier. A creation of a positively charged circular region will exert attractive downward forces on the nanoparticle, counterbalancing the repulsive upward forces and therefore reducing the free energy barrier. This effect will become larger as the area of the positively charged circular region increases. As an example, the influence of the circular diameter on the interaction force landscape and interaction free energy barrier is shown in Figure 9 for the case of IS = 0.05 mM and $\sigma_{NP} = -1.5 \,\mu\text{C/cm}^2$ with no nanoparticle present at the circle center. We observe stronger upward forces for d = 100 nm (Figure 9a) than for d =150 nm (Figure 9b). In particular, for d = 100 nm, even if the nanoparticle is positioned more than 100 nm above the circular template, substantial upward forces exist (see the forces inside the red dashed circle in Figure 9a). On the other hand, for d = 150 nm, the upward forces are substantially reduced or even reversed to the downward direction (see the forces inside the red dashed circle in Figure 9b) due to the larger positively charged circular area on the substrate surface. For the former (d = 100 nm), those repulsive forces lead to a substantial interaction free energy barrier (0.362 eV), but for the latter (d = 150 nm), the substantially reduced repulsive forces lead to a much smaller interaction free energy barrier (0.087 eV). This clear difference in the free energy behaviors is shown in the interaction free energy plot in Figure 9c.

Suitable Parameter Space for SPP. The effects of ionic strengths, nanoparticle surface charge densities, and circle diameters on the interaction free energy barriers can be collectively displayed using 3-dimensional plots, where the interaction free energy barriers are displayed in the z-axis at different ionic strengths and nanoparticle surface charge densities (x and y axes). Figure 10a,b shows those plots for d = 100 nm and d = 150 nm, respectively [(i,ii): without and with a nanoparticle at the circle center, respectively]. The numerical values of the interaction free energy barriers are also provided in the tables below the 3-D plots. The two free energy barrier criteria (i.e., ≤0.2 and >1.25 eV, without and with a nanoparticle at the circle center, respectively) are used to identify the right sets of ionic strengths and nanoparticle surface charge densities at given circle diameters. In Figure 10, we have highlighted the parameter sets in three different colors in the 3-D plots as well as the corresponding tables as follows. The greens represent that the parameter sets satisfy both criteria. The reds represent that the parameter sets do not satisfy the first criterion (\leq 0.2 eV) for the case that there is no nanoparticle at the circle center [Figure 10a(i),b(i)] or do not satisfy the second criterion (>1.25 eV) for the case that there is a nanoparticle at the circle center [Figure 10a(ii),b(ii)]. Yellows represent that the parameter sets satisfy only one of the two criteria. For example, a parameter set of (IS, σ_{NP} , d) = $(0.5 \text{ mM}, -1.5 \mu\text{C/cm}^2, 100 \text{ nm})$ leads to free energy barriers of 0.008 and 1.722 eV without and with a nanoparticle at the circle center, respectively, which satisfy both criteria, and therefore, this set is highlighted in green in both Figure 10a(i,ii). On the other hand, the set of (IS, $\sigma_{\rm NP}$, d) = (0.5 mM, $-0.3 \mu \text{C/cm}^2$, 100 nm) leads to free energy barriers of 0.001 and 0.151 eV without and with a nanoparticle at the circle center, respectively. The former (0.001 eV) satisfies the first criterion (\leq 0.2 eV), but the latter (0.151 eV) does not satisfy the second criterion (>1.25 eV), which are represented in yellow in Figure 10a(i) and in red in Figure 10a(ii), respectively. From these representations, the suitable parameter sets that satisfy both criteria are easily distinguishable by the highlights in green in the 3-D plots as well as in the corresponding tables in Figure 10. From the red and yellow domains, it can be concluded that the magnitude of the

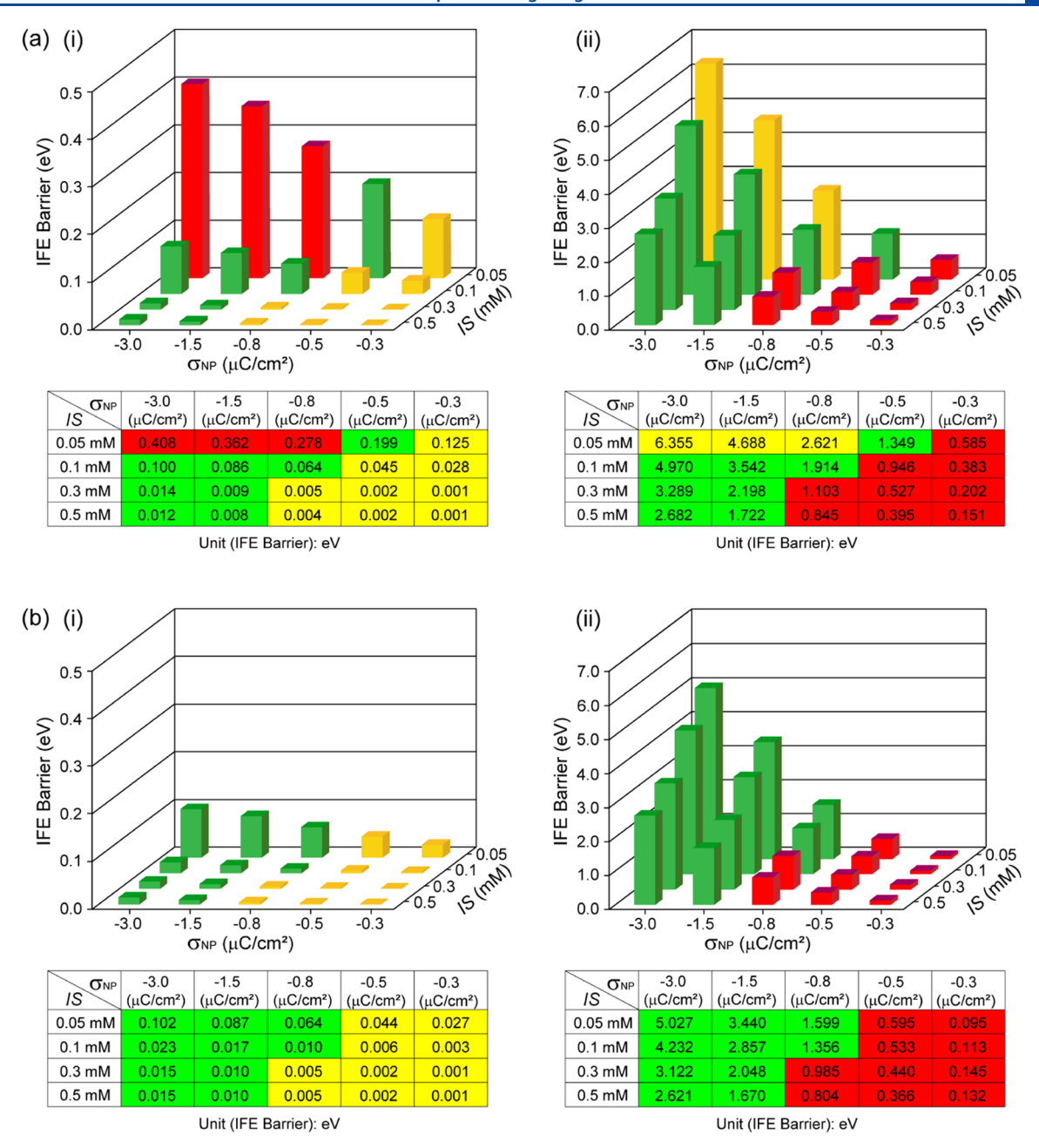


Figure 10. Interaction free energy barriers for differing nanoparticle surface charge densities and ionic strengths. (a) For d = 100 nm. (b) For d = 150 nm. (i,ii) Without and with a nanoparticle at the circle center, respectively. IFE barrier criteria: ≤ 0.2 and >1.25 eV, without and with a nanoparticle at the circle center, respectively. Greens represent both criteria are met. Yellows represent only one criterion is met. Reds represent the parameter sets do not satisfy the first criterion (≤ 0.2 eV) for the case that there is no nanoparticle at the circle center or do not satisfy the second criterion (>1.25 eV) for the case that there is a nanoparticle at the circle center.

nanoparticle surface charge density $\sigma_{\rm NP}$ should be at least 0.5 $\mu{\rm C/cm^2}$ when d=100 nm and 0.8 $\mu{\rm C/cm^2}$ when d=150 nm. The green domains in Figure 10 provide ranges of parameter sets that can be used in experiments for successful SPP.

The parameter landscape in Figure 10 suggests that a variety of nanoparticle placements could be realized by cleverly selecting appropriate parameter sets in SPP. For example, it would be possible to selectively place two different species of nanoparticles (e.g., Au and Ag nanoparticles) onto two different kinds of locations; for example, α nanoparticles are placed on α locations and β nanoparticles are placed on β locations. This species-specific single-nanoparticle placement can be realized as follows. A substrate can be prepared with

circular templates of two different diameters, $d_{\alpha}=150$ nm and $d_{\beta}=100$ nm, positioned at α and β locations, respectively. Assuming that both α and β nanoparticles have a surface charge density of $-0.8~\mu\text{C/cm}^2$, if a colloid of α nanoparticles in an ionic strength of 0.05 mM is applied to the substrate, they will be placed only on the circular templates of $d_{\alpha}=150$ nm [IFE barrier 0.064 eV, see Figure 10b(i)], but rejected from circular templates of $d_{\beta}=100$ nm [IFE barrier 0.278 eV, see Figure 10a(i)]. After washing, a colloid of β nanoparticles in an ionic strength of 0.1 mM can be applied, which will allow the placement of β nanoparticles on the circular templates of $d_{\beta}=100$ nm [IFE barrier 0.064 eV, see Figure 10a(i)]. No β nanoparticles can be placed on α locations because they are

already occupied by α nanoparticles from the previous step, enabling species-specific single-nanoparticle placement. The above is just one example where the effect of the template diameter is utilized but a much richer parameter landscape and associated applications will emerge if more parameter ranges are explored. For example, surface charge densities σ_{circle} and $\sigma_{\text{substrate}}$ of the circular template and substrate surface, which were fixed in this study, can be varied over a large range by forming SAMs of mixed molecules in various ratios. The enriched realms of the parameter space that enable SPP would allow well-controlled single-nanoparticle placement that can be tailored for specific nanoparticles and applications.

The self-limiting SPP can be applied for any nanoparticles (e.g., metal, semiconducting, non-conducting, and magnetic nanoparticles) as long as they are adequately charged. The SPP concept may also be applied to placing single nanowires on exact substrate positions, using rectangular, rather than circular, templates to electrostatically guide the single nanowires. The capability of placing these nanoscale building blocks on a single-entity level, on a large scale, and with nanoscale precision has been long sought as it is a critical element for the bottom-up construction of various novel devices and sensors. The SPP method can provide such capability. In particular, its large-scale and large-area placement capability (due to the capability of defining the templates on a wafer scale using CMOS-compatible processes and materials) could pave a way toward the practical fabrication of such devices and sensors.

The future work may include extending the current study and creating a comprehensive phase diagram that predicts whether a specific parameter set of arbitrary values [e.g., (IS, $\sigma_{\rm NP}$, d) = (0.12 mM, -0.93 $\mu{\rm C/cm^2}$, 117 nm)] leads to a successful SPP or not. The phase diagram will be in 3D as there are three independent parameters (i.e., IS, σ_{NP} , and d). Constructing such a phase diagram would demand substantial computational time and cost, and therefore would require a methodology that can cost-effectively calculate the phase diagram with a good accuracy. One strategy we may consider is a two-stage calculation, in which a phase diagram with discrete parameter values (e.g., $\sigma_{NP} = -3.0, -1.5, -0.8, -0.5, \text{ and } -0.3$ μ C/cm²) is first obtained and then the final phase diagram with fine-tuned parameter values is obtained subsequently. The former is simply a 3-dimensional parameter region, with discrete boundaries, that satisfies both IFE barrier criteria. Then, the bisection method is applied only near the boundaries to obtain the fine-tuned phase diagram. For example, let us assume that (IS*, σ_{NP}^* , d^*) is a (discrete) parameter set at the boundary of the initial phase diagram. We evaluate whether a set (IS*, $\sigma_{NP}^* + \delta \sigma_{NP}$, d^*) satisfies the two IFE barrier criteria or not. In the case that it does not, we know that the true boundary is located between (IS*, $\sigma_{\rm NP}$ * + $\delta\sigma_{\rm NP}$, d^*) and (IS*, $\sigma_{\rm NP}$ *, d^*). We then evaluate if (IS*, $\sigma_{\rm NP}$ * + $\delta\sigma_{\rm NP}/2$, d^*) satisfies the two IFE barrier criteria. Such an evaluation is continued until we fine-tune the boundary of $\sigma_{
m NP}$ with a predefined accuracy. With the same procedure, the boundaries of IS and d are also fine-tuned. The above are carried out for finite sets of (IS*, σ_{NP}^* , d^*)'s (a compromise between computational cost and resolution) and proper interpolations are used to produce the final phase diagram.

CONCLUSIONS

This study has numerically investigated the effects of the following three parameters on the self-limiting SPP: (1) ionic strength (IS) of the colloid, (2) nanoparticle surface charge

density $(\sigma_{\rm NP})$, and (3) the diameter (d) of a circular template. The parameter values explored were (1) 0.5, 0.3, 0.1, and 0.05 mM for IS; (2) -3.0, -1.5, -0.8, -0.5, and $-0.3~\mu{\rm C/cm^2}$ for $\sigma_{\rm NP}$; and (3) 100 and 150 nm for d. A total of 40 (= $4\times5\times2$) different parameter sets were explored to study their roles on SPP. A 30 nm nanoparticle positioned at \vec{R} above the substrate was modeled in two geometrical configurations, (i) without and (ii) with a 30 nm nanoparticle at the center of a circular template. For each parameter set $(IS, \sigma_{\rm NP}, d)$, \vec{R} , and geometrical configuration, the electrostatic potentials $\psi(\vec{r})$ were calculated by numerically solving the PBE, from which the interaction force exerted on the nanoparticle at \vec{R} and the interaction free energy were calculated.

The values of the interaction free energies (IFEs) and IFE barriers are used to assess the effects of the three parameters, IS, $\sigma_{\rm NP}$, and d, on SPP. It is found that as the ionic strengths (ISs) decrease from 0.5 to 0.05 mM, the IFE and IFE barriers increase for given $\sigma_{\rm NP}$ and d. As the magnitudes of the nanoparticle surface charge densities decrease from 3.0 to 0.3 $\mu{\rm C/cm^2}$, the IFE and IFE barriers decrease for given IS and d. As the diameter d of the circular template increases from 100 to 150 nm, the IFE and IFE barriers decrease for given IS and $\sigma_{\rm NP}$.

To quantitatively identify the parameter sets (IS, σ_{NP} , d) for successful SPP, two IFE barrier criteria have been set, ≤0.2 and >1.25 eV for the cases of (i) without and (ii) with a nanoparticle at the center of the circular template, respectively. For a circular diameter of 100 nm, the parameter sets are (IS, $\sigma_{\rm NP}$, d) = (0.5 mM, -3.0 μ C/cm², 100 nm), (0.5 mM, -1.5 μ C/cm², 100 nm), (0.3 mM, -3.0 μ C/cm², 100 nm), (0.3 mM, $-1.5 \mu \text{C/cm}^2$, 100 nm), (0.1 mM, $-3.0 \mu \text{C/cm}^2$, 100 nm), (0.1 mM, $-1.5 \mu \text{C/cm}^2$, 100 nm), (0.1 mM, $-0.8 \mu \text{C/cm}^2$ cm², 100 nm), and (0.05 mM, $-0.5 \mu C/cm^2$, 100 nm). For a circle diameter of 150 nm, they are (IS, σ_{ND} , d) = (0.5 mM, $-3.0 \ \mu\text{C/cm}^2$, 150 nm), (0.5 mM, $-1.5 \ \mu\text{C/cm}^2$, 150 nm), $(0.3 \text{ mM}, -3.0 \mu\text{C/cm}^2, 150 \text{ nm}), (0.3 \text{ mM}, -1.5 \mu\text{C/cm}^2)$ 150 nm), (0.1 mM, $-3.0 \mu \text{C/cm}^2$, 150 nm), (0.1 mM, -1.5 μ C/cm², 150 nm), (0.1 mM, -0.8μ C/cm², 150 nm), (0.05 mM, $-3.0 \ \mu\text{C/cm}^2$, 150 nm), (0.05 mM, $-1.5 \ \mu\text{C/cm}^2$, 150 nm), and (0.05 mM, $-0.8 \mu C/cm^2$, 150 nm). These indicate that, for the parameter space explored, a necessary condition for a successful SPP is that the magnitude of the nanoparticle surface charge density should be 0.5 μ C/cm² or above for d =100 nm and 0.8 μ C/cm² or above for d = 150 nm.

This numerical study identifies the realms of the (IS, $\sigma_{\rm NP}$, d)-parameter space for successful SPP. Its findings can be used to guide experiments for large-scale and large-area placements of single nanoparticles, paving a way toward bottom-up constructions of novel devices and sensors using nanoscale building blocks.

ASSOCIATED CONTENT

Supporting Information

The Supporting Information is available free of charge at https://pubs.acs.org/doi/10.1021/acs.langmuir.1c01375.

Relationship between surface charge densities and Stern potentials for the nanoparticle, circular template, and substrate surface; figure displaying the nanoparticle positions \vec{R} 's used in this study; calculated interaction forces exerted on a single nanoparticle at varying ionic strengths, nanoparticle surface charge densities, and circle diameters; and constant potential (CP) and

constant charge (CC) boundary conditions in solving the PBE (PDF)

AUTHOR INFORMATION

Corresponding Author

Seong Jin Koh – Department of Materials Science and Engineering, University of Texas at Arlington, Arlington, Texas 76019, United States; orcid.org/0000-0001-7721-5593; Email: skoh@uta.edu

Authors

Pushkar K. Gothe — Department of Materials Science and Engineering, University of Texas at Arlington, Arlington, Texas 76019, United States; orcid.org/0000-0002-8471-3889

Anthony Martinez — Department of Materials Science and Engineering, University of Texas at Arlington, Arlington, Texas 76019, United States; orcid.org/0000-0002-0624-4888

Complete contact information is available at: https://pubs.acs.org/10.1021/acs.langmuir.1c01375

Author Contributions

[†]P.K.G. and A.M. contributed equally. The manuscript was written through contributions of all authors. All authors have given approval to the final version of the manuscript.

Notes

The authors declare no competing financial interest.

ACKNOWLEDGMENTS

We thank N. Michael for critical reading of the manuscript. This work was supported by the National Science Foundation (ECCS-2031770, DMR-2122128, and CMMI-1463451).

ABBREVIATIONS

SPP, self-limiting single-particle placement; IS, ionic strength; IFE, interaction free energy; SAMs, self-assembled monolayers; APTES, 3-aminopropyltriethoxysilane; MHA, 16-mercaptohexadecanoic acid; PBE, Poisson-Boltzmann equations; OHP, outer Helmholtz plane; IHP, inner Helmholtz plane

REFERENCES

- (1) Banin, U.; Cao, Y.; Katz, D.; Millo, O. Identification of Atomic-Like Electronic States in Indium Arsenide Nanocrystal Quantum Dots. *Nature* **1999**, 400, 542–544.
- (2) Bhadrachalam, P.; Subramanian, R.; Ray, V.; Ma, L.-C.; Wang, W.; Kim, J.; Cho, K.; Koh, S. J. Energy-Filtered Cold Electron Transport at Room Temperature. *Nat. Commun.* **2014**, *5*, 4745.
- (3) Klein, D. L.; Roth, R.; Lim, A. K. L.; Alivisatos, A. P.; McEuen, P. L. A Single-Electron Transistor Made from a Cadmium Selenide Nanocrystal. *Nature* **1997**, 389, 699–701.
- (4) Ray, V.; Subramanian, R.; Bhadrachalam, P.; Ma, L.-C.; Kim, C.-U.; Koh, S. J. CMOS-Compatible Fabrication of Room-Temperature Single-Electron Devices. *Nat. Nanotechnol.* **2008**, *3*, 603–608.
- (S) Overgaag, K.; Liljeroth, P.; Grandidier, B.; Vanmaekelbergh, D. Scanning Tunneling Spectroscopy of Individual PbSe Quantum Dots and Molecular Aggregates Stabilized in an Inert Nanocrystal Matrix. ACS Nano 2008, 2, 600–606.
- (6) Makarenko, K. S.; Liu, Z.; de Jong, M. P.; Zwanenburg, F. A.; Huskens, J.; van der Wiel, W. G. Bottom-Up Single-Electron Transistors. *Adv. Mater.* **2017**, *29*, 1702920.
- (7) Bitton, O.; Gutman, D. B.; Berkovits, R.; Frydman, A. Multiple Periodicity in a Nanoparticle-Based Single-Electron Transistor. *Nat. Commun.* **2017**, *8*, 402.

- (8) Azuma, Y.; Sakamoto, M.; Teranishi, T.; Majima, Y. Memory Operations in Au Nanoparticle Single-Electron Transistors with Floating Gate Electrodes. *Appl. Phys. Lett.* **2016**, *109*, 223106.
- (9) Temple, R. C.; McLaren, M.; Brydson, R. M. D.; Hickey, B. J.; Marrows, C. H. Long Spin Lifetime and Large Barrier Polarisation in Single Electron Transport Through a CoFe Nanoparticle. *Sci. Rep.* **2016**, *6*, 28296.
- (10) Michler, P.; Kiraz, A.; Becher, C.; Schoenfeld, W. V.; Petroff, P. M.; Zhang, L. D.; Hu, E.; Imamoglu, A. A Quantum Dot Single-Photon Turnstile Device. *Science* **2000**, *290*, 2282–2285.
- (11) Elshaari, A. W.; Zadeh, I. E.; Fognini, A.; Reimer, M. E.; Dalacu, D.; Poole, P. J.; Zwiller, V.; Jöns, K. D. On-Chip Single Photon Filtering and Multiplexing in Hybrid Quantum Photonic Circuits. *Nat. Commun.* **2017**, *8*, 379.
- (12) Müller, M.; Bounouar, S.; Jöns, K. D.; Glässl, M.; Michler, P. On-Demand Generation of Indistinguishable Polarization-Entangled Photon Pairs. *Nat. Photonics* **2014**, *8*, 224–228.
- (13) Jones, M. R.; Osberg, K. D.; Macfarlane, R. J.; Langille, M. R.; Mirkin, C. A. Templated Techniques for the Synthesis and Assembly of Plasmonic Nanostructures. *Chem. Rev.* **2011**, *111*, 3736–3827.
- (14) Oh, J.-H.; Park, D. H.; Joo, J. H.; Lee, J.-S. Recent Advances in Chemical Functionalization of Nanoparticles with Biomolecules for Analytical Applications. *Anal. Bioanal. Chem.* **2015**, 407, 8627–8645.
- (15) Kovalenko, M. V.; Manna, L.; Cabot, A.; Hens, Z.; Talapin, D. V.; Kagan, C. R.; Klimov, V. I.; Rogach, A. L.; Reiss, P.; Milliron, D. J.; Guyot-Sionnnest, P.; Konstantatos, G.; Parak, W. J.; Hyeon, T.; Korgel, B. A.; Murray, C. B.; Heiss, W. Prospects of Nanoscience with Nanocrystals. *ACS Nano* **2015**, *9*, 1012–1057.
- (16) Zanoli, L. M.; D'Agata, R.; Spoto, G. Functionalized Gold Nanoparticles for Ultrasensitive DNA Detection. *Anal. Bioanal. Chem.* **2012**, 402, 1759–1771.
- (17) Maier, S. A.; Kik, P. G.; Atwater, H. A.; Meltzer, S.; Harel, E.; Koel, B. E.; Requicha, A. A. G. Local Detection of Electromagnetic Energy Transport Below the Diffraction Limit in Metal Nanoparticle Plasmon Waveguides. *Nat. Mater.* **2003**, *2*, 229–232.
- (18) Maier, S. A.; Atwater, H. A. Plasmonics: Localization and Guiding of Electromagnetic Energy in Metal/Dielectric Structures. *J. Appl. Phys.* **2005**, *98*, 011101.
- (19) Schuller, J. A.; Barnard, E. S.; Cai, W.; Jun, Y. C.; White, J. S.; Brongersma, M. L. Plasmonics for Extreme Light Concentration and Manipulation. *Nat. Mater.* **2010**, *9*, 193.
- (20) Gramotnev, D. K.; Bozhevolnyi, S. I. Plasmonics Beyond the Diffraction Limit. *Nat. Photonics* **2010**, *4*, 83.
- (21) Lan, X.; Wang, Q. Self-Assembly of Chiral Plasmonic Nanostructures. *Adv. Mater.* **2016**, 28, 10499–10507.
- (22) Golze, S. D.; Hughes, R. A.; Rouvimov, S.; Neal, R. D.; Demille, T. B.; Neretina, S. Plasmon-Mediated Synthesis of Periodic Arrays of Gold Nanoplates Using Substrate-Immobilized Seeds Lined with Planar Defects. *Nano Lett.* **2019**, *19*, 5653–5660.
- (23) Demille, T. B.; Hughes, R. A.; Dominique, N.; Olson, J. E.; Rouvimov, S.; Camden, J. P.; Neretina, S. Large-Area Periodic Arrays of Gold Nanostars Derived from HEPES-, DMF-, and Ascorbic-Acid-Driven Syntheses. *Nanoscale* **2020**, *12*, 16489–16500.
- (24) Noginov, M. A.; Zhu, G.; Belgrave, A. M.; Bakker, R.; Shalaev, V. M.; Narimanov, E. E.; Stout, S.; Herz, E.; Suteewong, T.; Wiesner, U. Demonstration of a Spaser-Based Nanolaser. *Nature* **2009**, *460*, 1110
- (25) Stockman, M. I. Spasers Explained. Nat. Photonics 2008, 2, 327.
- (26) Zheludev, N. I.; Prosvirnin, S. L.; Papasimakis, N.; Fedotov, V. A. Lasing Spaser. *Nat. Photonics* **2008**, *2*, 351.
- (27) Kuznetsov, A. I.; Miroshnichenko, A. E.; Fu, Y. H.; Zhang, J.; Luk'yanchuk, B. Magnetic Light. Sci. Rep. 2012, 2, 492.
- (28) Zaza, C.; Violi, I. L.; Gargiulo, J.; Chiarelli, G.; Schumacher, L.; Jakobi, J.; Olmos-Trigo, J.; Cortes, E.; König, M.; Barcikowski, S.; Schlücker, S.; Sáenz, J. J.; Maier, S. A.; Stefani, F. D. Size-Selective Optical Printing of Silicon Nanoparticles through Their Dipolar Magnetic Resonance. ACS Photonics 2019, 6, 815–822.
- (29) Li, W.; Liu, Y.; Wu, M.; Feng, X.; Redfern, S. A. T.; Shang, Y.; Yong, X.; Feng, T.; Wu, K.; Liu, Z.; Li, B.; Chen, Z.; Tse, J. S.; Lu, S.;

- Yang, B. Carbon-Quantum-Dots-Loaded Ruthenium Nanoparticles as an Efficient Electrocatalyst for Hydrogen Production in Alkaline Media. *Adv. Mater.* **2018**, *30*, 1800676.
- (30) Koh, S. Strategies for Controlled Placement of Nanoscale Building Blocks. *Nanoscale Res. Lett.* **2007**, *2*, 519–545.
- (31) Zhang, J.; Li, Y.; Zhang, X.; Yang, B. Colloidal Self-Assembly Meets Nanofabrication: From Two-Dimensional Colloidal Crystals to Nanostructure Arrays. *Adv. Mater.* **2010**, *22*, 4249–4269.
- (32) Hughes, R. A.; Menumerov, E.; Neretina, S. When Lithography Meets Self-Assembly: A Review of Recent Advances in the Directed Assembly of Complex Metal Nanostructures on Planar and Textured Surfaces. *Nanotechnology* **2017**, *28*, 282002.
- (33) Yin, Y.; Lu, Y.; Xia, Y. A Self-Assembly Approach to the Formation of Asymmetric Dimers from Monodispersed Spherical Colloids. J. Am. Chem. Soc. 2001, 123, 771–772.
- (34) Lee, J. B.; Walker, H.; Li, Y.; Nam, T. W.; Rakovich, A.; Sapienza, R.; Jung, Y. S.; Nam, Y. S.; Maier, S. A.; Cortés, E. Template Dissolution Interfacial Patterning of Single Colloids for Nanoelectrochemistry and Nanosensing. *ACS Nano* **2020**, *14*, 17693–17703.
- (35) Flauraud, V.; Mastrangeli, M.; Bernasconi, G. D.; Butet, J.; Alexander, D. T. L.; Shahrabi, E.; Martin, O. J. F.; Brugger, J. Nanoscale Topographical Control of Capillary Assembly of Nanoparticles. *Nat. Nanotechnol.* **2017**, *12*, 73–80.
- (36) Jiang, W.; Ma, Y.; Zhao, J.; Li, L.; Xu, Y.; Guo, H.; Song, L.; Chen, Z.; Zhang, Y. Robust Assembly of Colloidal Nanoparticles for Controlled-Reflectance Surface Construction. ACS Appl. Mater. Interfaces 2019, 11, 23773–23779.
- (37) Liberman, V.; Yilmaz, C.; Bloomstein, T. M.; Somu, S.; Echegoyen, Y.; Busnaina, A.; Cann, S. G.; Krohn, K. E.; Marchant, M. F.; Rothschild, M. A Nanoparticle Convective Directed Assembly Process for the Fabrication of Periodic Surface Enhanced Raman Spectroscopy Substrates. *Adv. Mater.* **2010**, *22*, 4298–4302.
- (38) Ma, L.-C.; Subramanian, R.; Huang, H.-W.; Ray, V.; Kim, C.-U.; Koh, S. J. Electrostatic Funneling for Precise Nanoparticle Placement: A Route to Wafer-Scale Integration. *Nano Lett.* **2007**, *7*, 439–445.
- (39) Huang, H.-W.; Bhadrachalam, P.; Ray, V.; Koh, S. J. Single-Particle Placement via Self-Limiting Electrostatic Gating. *Appl. Phys. Lett.* **2008**, 93, 073110.
- (40) Yoshii, S.; Kumagai, S.; Nishio, K.; Kadotani, A.; Yamashita, I. Electrostatic Self-Aligned Placement of Single Nanodots by Protein Supramolecules. *Appl. Phys. Lett.* **2009**, *95*, 133702.
- (41) Lin, M.-H.; Chen, C.-F.; Shiu, H.-W.; Chen, C.-H.; Gwo, S. Multilength-Scale Chemical Patterning of Self-Assembled Monolayers by Spatially Controlled Plasma Exposure: Nanometer to Centimeter Range. J. Am. Chem. Soc. 2009, 131, 10984–10991.
- (42) Nepal, D.; Onses, M. S.; Park, K.; Jespersen, M.; Thode, C. J.; Nealey, P. F.; Vaia, R. A. Control over Position, Orientation, and Spacing of Arrays of Gold Nanorods Using Chemically Nanopatterned Surfaces and Tailored Particle-Particle-Surface Interactions. *ACS Nano* **2012**, *6*, 5693–5701.
- (43) Lloyd, J. A.; Liu, Y.; Ng, S. H.; Thai, T.; Gómez, D. E.; Widmer-Cooper, A.; Bach, U. Self-Assembly of Spherical and Rod-Shaped Nanoparticles with Full Positional Control. *Nanoscale* **2019**, *11*, 22841–22848.
- (44) Lloyd, J. A.; Ng, S. H.; Davis, T. J.; Gómez, D. E.; Bach, U. Size Selective Adsorption of Gold Nanoparticles by Electrostatic Assembly. *J. Phys. Chem. C* **2017**, *121*, 2437–2443.
- (45) Carroll, K. M.; Wolf, H.; Knoll, A.; Curtis, J. E.; Zhang, Y.; Marder, S. R.; Riedo, E.; Duerig, U. Understanding How Charged Nanoparticles Electrostatically Assemble and Distribute in 1-D. *Langmuir* **2016**, *32*, 13600–13610.
- (46) Morakinyo, M. K.; Rananavare, S. B. Reducing the Effects of Shot Noise Using Nanoparticles. *J. Mater. Chem. C* **2015**, *3*, 955–959.
- (47) Nidetz, R.; Kim, J. Directed Self-Assembly of Nanogold Using a Chemically Modified Nanopatterned Surface. *Nanotechnology* **2012**, 23, 045602.

- (48) Zheng, Y.; Rosa, L.; Thai, T.; Ng, S. H.; Gómez, D. E.; Ohshima, H.; Bach, U. Asymmetric Gold Nanodimer Arrays: Electrostatic Self-Assembly and SERS Activity. *J. Mater. Chem. A* **2015**, 3, 240–249.
- (49) Fetterly, C. R.; Olsen, B. C.; Luber, E. J.; Buriak, J. M. Vapor-Phase Nanopatterning of Aminosilanes with Electron Beam Lithography: Understanding and Minimizing Background Functionalization. *Langmuir* **2018**, *34*, 4780–4792.
- (50) Kim, H.; Kim, J.; Yang, H.; Suh, J.; Kim, T.; Han, B.; Kim, S.; Kim, D. S.; Pikhitsa, P. V.; Choi, M. Parallel Patterning of Nanoparticles via Electrodynamic Focusing of Charged Aerosols. *Nat. Nanotechnol.* **2006**, *1*, 117–121.
- (51) Zhang, H.; Liu, Y.; Shahidan, M. F. S.; Kinnear, C.; Maasoumi, F.; Cadusch, J.; Akinoglu, E. M.; James, T. D.; Widmer-Cooper, A.; Roberts, A.; Mulvaney, P. Direct Assembly of Vertically Oriented, Gold Nanorod Arrays. *Adv. Funct. Mater.* **2021**, *31*, 2006753.
- (52) Kinnear, C.; Cadusch, J.; Zhang, H.; Lu, J.; James, T. D.; Roberts, A.; Mulvaney, P. Directed Chemical Assembly of Single and Clustered Nanoparticles with Silanized Templates. *Langmuir* **2018**, 34, 7355–7363.
- (53) Guffey, M. J.; Scherer, N. F. All-Optical Patterning of Au Nanoparticles on Surfaces Using Optical Traps. *Nano Lett.* **2010**, *10*, 4302–4308.
- (54) Guffey, M. J.; Miller, R. L.; Gray, S. K.; Scherer, N. F. Plasmon-Driven Selective Deposition of Au Bipyramidal Nanoparticles. *Nano Lett.* **2011**, *11*, 4058–4066.
- (55) Alam, M. S.; Zhan, Q.; Zhao, C. Additive Opto-Thermomechanical Nanoprinting and Nanorepairing under Ambient Conditions. *Nano Lett.* **2020**, *20*, 5057–5064.
- (56) Valuckas, V.; Paniagua-Domínguez, R.; Maimaiti, A.; Patra, P. P.; Wong, S. K.; Verre, R.; Käll, M.; Kuznetsov, A. I. Fabrication of Monodisperse Colloids of Resonant Spherical Silicon Nanoparticles: Applications in Optical Trapping and Printing. *ACS Photonics* **2019**, *6*, 2141–2148.
- (57) Gurunatha, K. L.; Fournier, A. C.; Urvoas, A.; Valerio-Lepiniec, M.; Marchi, V.; Minard, P.; Dujardin, E. Nanoparticles Self-Assembly Driven by High Affinity Repeat Protein Pairing. *ACS Nano* **2016**, *10*, 3176–3185.
- (58) Fernandez, M.; Urvoas, A.; Even-Hernandez, P.; Burel, A.; Mériadec, C.; Artzner, F.; Bouceba, T.; Minard, P.; Dujardin, E.; Marchi, V. Hybrid Gold Nanoparticle-Quantum Dot Self-Assembled Nanostructures Driven by Complementary Artificial Proteins. *Nanoscale* 2020, 12, 4612–4621.
- (59) Benn, F.; Haley, N. E. C.; Lucas, A. E.; Silvester, E.; Helmi, S.; Schreiber, R.; Bath, J.; Turberfield, A. J. Chiral DNA Origami Nanotubes with Well-Defined and Addressable Inside and Outside Surfaces. *Angew. Chem., Int. Ed.* **2018**, *57*, 7687–7690.
- (60) Gür, F. N.; Schwarz, F. W.; Ye, J.; Diez, S.; Schmidt, T. L. Toward Self-Assembled Plasmonic Devices: High-Yield Arrangement of Gold Nanoparticles on DNA Origami Templates. *ACS Nano* **2016**, 10, 5374–5382.
- (61) Lalander, C. H.; Zheng, Y.; Dhuey, S.; Cabrini, S.; Bach, U. DNA-Directed Self-Assembly of Gold Nanoparticles onto Nanopatterned Surfaces: Controlled Placement of Individual Nanoparticles into Regular Arrays. ACS Nano 2010, 4, 6153–6161.
- (62) Čecconello, A.; Simmel, F. C. Controlling Chirality across Length Scales using DNA. *Small* **2019**, *15*, 1805419.
- (63) Bang, J.; Jeong, U.; Ryu, D. Y.; Russell, T. P.; Hawker, C. J. Block Copolymer Nanolithography: Translation of Molecular Level Control to Nanoscale Patterns. *Adv. Mater.* **2009**, *21*, 4769–4792.
- (64) Yan, N.; Liu, X.; Zhu, J.; Zhu, Y.; Jiang, W. Well-Ordered Inorganic Nanoparticle Arrays Directed by Block Copolymer Nanosheets. ACS Nano 2019, 13, 6638–6646.
- (65) Saini, A.; Theis-Bröhl, K.; Koutsioubas, A.; Krycka, K. L.; Borchers, J. A.; Wolff, M. Magnetic Particle Self-Assembly at Functionalized Interfaces. *Langmuir* **2021**, *37*, 4064–4071.
- (66) Nikolay, N.; Sadzak, N.; Dohms, A.; Lubotzky, B.; Abudayyeh, H.; Rapaport, R.; Benson, O. Accurate Placement of Single

- Nanoparticles on Opaque Conductive Structures. Appl. Phys. Lett. 2018, 113, 113107.
- (67) Kim, J.-H.; Aghaeimeibodi, S.; Richardson, C. J. K.; Leavitt, R. P.; Englund, D.; Waks, E. Hybrid Integration of Solid-State Quantum Emitters on a Silicon Photonic Chip. *Nano Lett.* **2017**, *17*, 7394–7400
- (68) Osada, A.; Ota, Y.; Katsumi, R.; Kakuda, M.; Iwamoto, S.; Arakawa, Y. Strongly Coupled Single-Quantum-Dot-Cavity System Integrated on a CMOS-Processed Silicon Photonic Chip. *Phys. Rev. Appl.* **2019**, *11*, 024071.
- (69) Ziefuß, A. R.; Haxhiaj, I.; Muller, S.; Gharib, M.; Gridina, O.; Rehbock, C.; Chakraborty, I.; Peng, B. X.; Muhler, M.; Parak, W. J.; Barcikowski, S.; Reichenberger, S. Origin of Laser-Induced Colloidal Gold Surface Oxidation and Charge Density, and Its Role in Oxidation Catalysis. *J. Phys. Chem. C* 2020, 124, 20981–20990.
- (70) Alan, B. O.; Barisik, M.; Ozcelik, H. G. Roughness Effects on the Surface Charge Properties of Silica Nanoparticles. *J. Phys. Chem. C* **2020**, 124, 7274–7286.
- (71) Brown, M. A.; Abbas, Z.; Kleibert, A.; Green, R. G.; Goel, A.; May, S.; Squires, T. M. Determination of Surface Potential and Electrical Double-Layer Structure at the Aqueous Electrolyte-Nanoparticle Interface. *Phys. Rev. X* **2016**, *6*, 011007.
- (72) Yakin, F. E.; Barisik, M.; Sen, T. Pore Size and Porosity Dependent Zeta Potentials of Mesoporous Silica Nanoparticles. *J. Phys. Chem. C* **2020**, *124*, 19579–19587.
- (73) Israelachvili, J. N. Intermolecular and Surface Forces, 3rd ed.; Academic Press: London, 2011.
- (74) Yamada, K.; Yoshii, S.; Kumagai, S.; Fujiwara, I.; Nishio, K.; Okuda, M.; Matsukawa, N.; Yamashita, I. High-Density and Highly Surface Selective Adsorption of Protein-Nanoparticle Complexes by Controlling Electrostatic Interaction. *Jpn. J. Appl. Phys.* **2006**, *45*, 4259–4264.
- (75) Schweiss, R.; Pleul, D.; Simon, F.; Janke, A.; Welzel, P. B.; Voit, B.; Knoll, W.; Werner, C. Electrokinetic Potentials of Binary Self-Assembled Monolayers on Gold: Acid—Base Reactions and Double Layer Structure. *J. Phys. Chem. B* **2004**, *108*, 2910—2917.
- (76) Schweiss, R.; Welzel, P. B.; Werner, C.; Knoll, W. Dissociation of Surface Functional Groups and Preferential Adsorption of Ions on Self-Assembled Monolayers Assessed by Streaming Potential and Streaming Current Measurements. *Langmuir* **2001**, *17*, 4304–4311.
- (77) Valtiner, M.; Banquy, X.; Kristiansen, K.; Greene, G. W.; Israelachvili, J. N. The Electrochemical Surface Forces Apparatus: The Effect of Surface Roughness, Electrostatic Surface Potentials, and Anodic Oxide Growth on Interaction Forces, and Friction between Dissimilar Surfaces in Aqueous Solutions. *Langmuir* **2012**, *28*, 13080–13093.
- (78) Kumagai, S.; Yoshii, S.; Yamada, K.; Matsukawa, N.; Fujiwara, I.; Iwahori, K.; Yamashita, I. Electrostatic Placement of Single Ferritin Molecules. *Appl. Phys. Lett.* **2006**, *88*, 153103.
- (79) Kane, V.; Mulvaney, P. Double-Layer Interactions between Self-Assembled Monolayers of ω-Mercaptoundecanoic Acid on Gold Surfaces. *Langmuir* **1998**, *14*, 3303–3311.
- (80) Adamczyk, Z.; Warszyński, P. Role of Electrostatic Interactions in Particle Adsorption. *Adv. Colloid Interface Sci.* **1996**, *63*, 41–149.
- (81) Stankovich, J.; Carnie, S. L. Electrical Double Layer Interaction between Dissimilar Spherical Colloidal Particles and between a Sphere and a Plate: Nonlinear Poisson—Boltzmann Theory. *Langmuir* 1996, 12, 1453—1461.
- (82) Warszynski, P.; Adamczyk, Z. Calculations of Double-Layer Electrostatic Interactions for the Sphere/Plane Geometry. *J. Colloid Interface Sci.* 1997, 187, 283–295.
- (83) Adamczyk, Z. Particle Adsorption and Deposition: Role of Electrostatic Interactions. *Adv. Colloid Interface Sci.* **2003**, 100–102, 267–347.
- (84) Bhattacharjee, S.; Elimelech, M. Surface Element Integration: A Novel Technique for Evaluation of DLVO Interaction Between a Particle and a Flat Plate. *J. Colloid Interface Sci.* **1997**, 193, 273–285.

- (85) Meegoda, J. N.; Hewage, S. A.; Batagoda, J. H. Application of the Diffused Double Layer Theory to Nanobubbles. *Langmuir* **2019**, 35, 12100–12112.
- (86) Dougherty, G. M.; Rose, K. A.; Tok, J. B.-H.; Pannu, S. S.; Chuang, F. Y. S.; Sha, M. Y.; Chakarova, G.; Penn, S. G. The Zeta Potential of Surface-Functionalized Metallic Nanorod Particles in Aqueous Solution. *Electrophoresis* **2008**, *29*, 1131–1139.
- (87) Lowry, G. V.; Hill, R. J.; Harper, S.; Rawle, A. F.; Hendren, C. O.; Klaessig, F.; Nobbmann, U.; Sayre, P.; Rumble, J. Guidance to improve the scientific value of zeta-potential measurements in nanoEHS. *Environ. Sci.: Nano* **2016**, *3*, 953–965.
- (88) Fawcett, W. R.; Fedurco, M.; Kovacova, Z. Double Layer Effects at Molecular Films Containing Acid/Base Groups. *Langmuir* **1994**, *10*, 2403–2408.
- (89) Kuo, C.-H.; Chang, H.-Y.; Liu, C.-P.; Lee, S.-H.; You, Y.-W.; Shyue, J.-J. Effect of Surface Chemical Composition on the Surface Potential and Iso-Electric Point of Silicon Substrates Modified with Self-Assembled Monolayers. *Phys. Chem. Chem. Phys.* **2011**, *13*, 3649–3653.
- (90) Hunter, S. J.; Penfold, N. J. W.; Chan, D. H.; Mykhaylyk, O. O.; Armes, S. P. How Do Charged End-Groups on the Steric Stabilizer Block Influence the Formation and Long-Term Stability of Pickering Nanoemulsions Prepared Using Sterically Stabilized Diblock Copolymer Nanoparticles? *Langmuir* **2020**, *36*, 769–780.
- (91) Huang, J.; Zajforoushan Moghaddam, S.; Maroni, P.; Thormann, E. Swelling Behavior, Interaction, and Electrostatic Properties of Chitosan/Alginate Dialdehyde Multilayer Films with Different Outermost Layer. *Langmuir* **2020**, *36*, 3782–3791.
- (92) Biggs, S.; Mulvaney, P.; Zukoski, C. F.; Grieser, F. Study of Anion Adsorption at the Gold-Aqueous Solution Interface by Atomic Force Microscopy. *J. Am. Chem. Soc.* **1994**, *116*, 9150–9157.
- (93) Markovich, T.; Andelman, D.; Podgornik, R. Charge Regulation: A Generalized Boundary Condition? *Epl* **2016**, *113*, 26004
- (94) Curk, T.; Luijten, E. Charge Regulation Effects in Nanoparticle Self-Assembly. *Phys. Rev. Lett.* **2021**, *126*, 138003.
- (95) Pericet-Camara, R.; Papastavrou, G.; Behrens, S. H.; Borkovec, M. Interaction between Charged Surfaces on the Poisson—Boltzmann Level: The Constant Regulation Approximation. *J. Phys. Chem. B* **2004**, *108*, 19467—19475.
- (96) Carnie, S. L.; Chan, D. Y. C.; Gunning, J. S. Electrical Double Layer Interaction between Dissimilar Spherical Colloidal Particles and between a Sphere and a Plate: The Linearized Poisson-Boltzmann Theory. *Langmuir* **1994**, *10*, 2993–3009.
- (97) Mazza, M. G.; Giovambattista, N.; Stanley, H. E.; Starr, F. W. Connection of Translational and Rotational Dynamical Heterogeneities with the Breakdown of the Stokes-Einstein and Stokes-Einstein-Debye Relations in Water. *Phys. Rev. E: Stat., Nonlinear, Soft Matter Phys.* 2007, 76, 031203.
- (98) Ohtori, N.; Ishii, Y. Explicit Expression for the Stokes-Einstein Relation for Pure Lennard-Jones Liquids. *Phys. Rev. E: Stat., Nonlinear, Soft Matter Phys.* **2015**, *91*, 012111.
- (99) Bhadra, P.; Siu, S. W. I. Effect of Concentration, Chain Length, Hydrophobicity, and an External Electric Field on the Growth of Mixed Alkanethiol Self-Assembled Monolayers: A Molecular Dynamics Study. *Langmuir* **2021**, *37*, 1913–1924.
- (100) Kong, G. D.; Song, H.; Yoon, S.; Kang, H.; Chang, R.; Yoon, H. J. Interstitially Mixed Self-Assembled Monolayers Enhance Electrical Stability of Molecular Junctions. *Nano Lett.* **2021**, *21*, 3162–3169.
- (101) Tricase, A.; Blasi, D.; Favia, A.; Stefanachi, A.; Leonetti, F.; Colafemmina, G.; Torsi, L.; Scamarcio, G. Surface Composition of Mixed Self-Assembled Monolayers on Au by Infrared Attenuated Total Reflection Spectroscopy. *Appl. Surf. Sci.* **2021**, *559*, 149883.
- (102) Blasi, D.; Sarcina, L.; Tricase, A.; Stefanachi, A.; Leonetti, F.; Alberga, D.; Mangiatordi, G. F.; Manoli, K.; Scamarcio, G.; Picca, R. A.; Torsi, L. Enhancing the Sensitivity of Biotinylated Surfaces by Tailoring the Design of the Mixed Self-Assembled Monolayer Synthesis. ACS Omega 2020, 5, 16762–16771.

(103) Ligorio, G.; Zorn Morales, N.; List-Kratochvil, E. J. W. Large and Continuous Tuning of the Work Function of Indium Tin Oxide Using Simple Mixing of Self-Assembled Monolayers. *Appl. Phys. Lett.* **2020**, *116*, 241603.